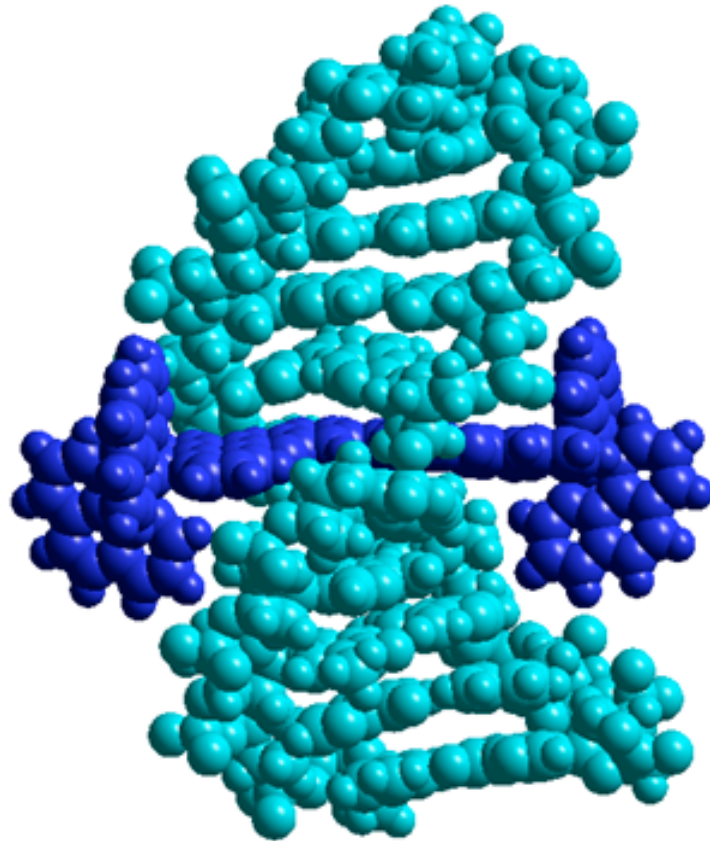


CHALMERS



Investigating how a crowded and hydrophobic environment
catalyzes DNA threading

Master of Science Thesis

IRFAN SHAUKAT

Department of Chemical and Biological Engineering
Division of Chemistry and Biochemistry
CHALMERS UNIVERSITY OF TECHNOLOGY
Göteborg, Sweden, 2011

THESIS FOR THE DEGREE OF MASTER OF SCIENCE

Investigating how a crowded and hydrophobic
environment catalyzes DNA threading

Irfan Shaukat



CHALMERS

Department of Chemical and Biological Engineering
CHALMERS UNIVERSITY OF TECHNOLOGY

Göteborg, Sweden, 2011

Investigating how a crowded and hydrophobic environment catalyzes DNA threading

Irfan Shukat

© Irfan Shukat, 2011

Department of Chemical and Biological Engineering
Chalmers University of Technology
SE-412 96 Göteborg
Sweden
Telephone +46 (0) 31-7200 1000

Cover picture:
Threading of $\Delta\Delta$ -P into DNA (explained in Figure 1.8)

Department of Chemical and Biological Engineering
Göteborg, Sweden, 2011

Investigating how a crowded and hydrophobic environment catalyzes DNA threading

Irfan Shuakat

Department of Chemical and Biological Engineering
Chalmers University of Technology

ABSTRACT

The intracellular environment is crowded due to the presence of biomacromolecules and other soluble and insoluble substances. Polyethylene glycol (PEG) is commonly used to mimic intracellular crowding *in vitro*. Recently it has been reported that PEG catalyzes DNA strand exchange. From this study it was not clear if the catalysis of PEG is due to crowding or hydrophobic interactions. Therefore we wanted a system which depends only on one of them.

Binuclear ruthenium complexes with general formula $[\mu\text{-bidppz}(\text{bipy})_4\text{Ru}_2]^{4+}$ (B), $[\mu\text{-bidppz}(\text{phen})_4\text{Ru}_2]^{4+}$ (P) have been extensively studied for their DNA threading property. The threading rate depends on the sequence of DNA as well as the structure and chirality of the ruthenium complex. Threading is believed to only depend on changes in water activity / hydrophobic interactions and not crowding. Thus if the threading is catalyzed by PEG this means that hydrophobic interactions are important in regards of the catalytic activity of PEG.

Threading into long mixed sequenced calf thymus DNA is very slow. 10% PEG catalyzes threading compared to aqueous buffer at all temperatures but higher PEG concentrations (20-30%) cause aggregation / precipitation of ct-DNA. Therefore we instead use a short synthetic oligonucleotide with a HEG-linked hairpin and a central AT track of 12 base pairs. There is significantly higher threading rate in 40% PEG compared to in buffer and the rate increases with increasing PEG concentration. DNA threading is more sensitive to PEG compared to DNA strand exchange. PEG has a larger catalytic effect on complex B compare to complex P. Therefore hydrophobic interactions are important for threading of the complex into DNA in a similar way as in the dissociation of the complex from DNA with sodium dodecyl sulfate (SDS).

Key words: DNA, ruthenium complexes, molecular crowding, fluorescence spectroscopy

List of abbreviations

Buffer	150 mM NaCl (1mM cacodylate, pH = 7)
bipy	2,2'-bipyridine
ct-DNA	<i>Calf thymus</i> DNA)
DNA	Deoxyribonucleic acid
HEG	Hexaethylene glycol
dppz	Dipyrido[3,2-a:2',3'-c]1.5 phenazine
LD	Linear Dichroism
MLCT	Metal-to-Ligand Charge Transfer
NaCl	Sodium Chloride
PEG	Polyethylene glycol
phen	1,10-N,N-Phenanthroline
RNA	Ribonucleic Acid
SDS	Sodium dodecyl sulphate
Δ	Right handed
Λ	Left handed

Table of Contents

1. Background	1
1.1 Structure of DNA	1
1.2 Metal based drugs and potential of ruthenium based drugs.....	3
1.3 Ruthenium Polypyridyl Complexes	5
1.4 Molecular Crowding	7
1.5 Objectives of our work	9
2. Fundamental concepts	10
2.1 UV-visible Spectroscopy	10
2.2 Fluorescence Spectroscopy	10
2.4 Linear dichroism (LD).....	12
3. Materials and Methods	13
3.1 PEG and Buffer.....	13
3.2 Ruthenium complexes.....	13
3.3 DNA models	13
3.4 Experimental setup	13
3.5 Instrumentation	14
3.6 Data Analysis	14
4. Results and Discussion	15
4.1 Calf thymus DNA and $\Delta\Delta$ -P.....	15
4.2 Calf thymus DNA and $\Lambda\Lambda$ -B	17
4.3 Linear dichroism of monomer and dimer complexes with ct-DNA.....	18
4.4 Temperature dependent threading rate in buffer and 10% PEG for ct-DNA.....	20
4.5 TA6 and $\Delta\Delta$ -P	20
4.6 Temperature dependent threading rate for TA6.....	22
5. Conclusions and outlook	25
Acknowledgement	27
Bibliography	28

1. Background

1.1 Structure of DNA

Deoxyribonucleic acid (DNA) is the hereditary material in almost all organisms. DNA was first discovered by the Swiss physician Friedrich Miescher as a microscopic substance from pus cells in 1869 and he called it "nuclein" [1]. In 1952, Hershey and Chase demonstrated that DNA is the heredity material [2]. Watson and Crick proposed the double-helix model of DNA in 1953 [3] and in 1962 they were awarded the Nobel Prize in physiology and medicine.

The central dogma of molecular biology, proposed by Crick in 1958 and published in Nature in 1970, [4] deals with the transfer of information from DNA into proteins (figure 1.1). The information in DNA is transcribed into mRNA and then mRNA is translated into proteins that perform different functions in the cells. DNA self replicates into DNA by DNA polymerases. In a specific process RNA can be converted to DNA by reverse transcription using reverse transcriptase. RNA can also be replicated by RNA dependent RNA polymerases. In cell free systems, DNA can act as messenger for production of proteins [5-6].

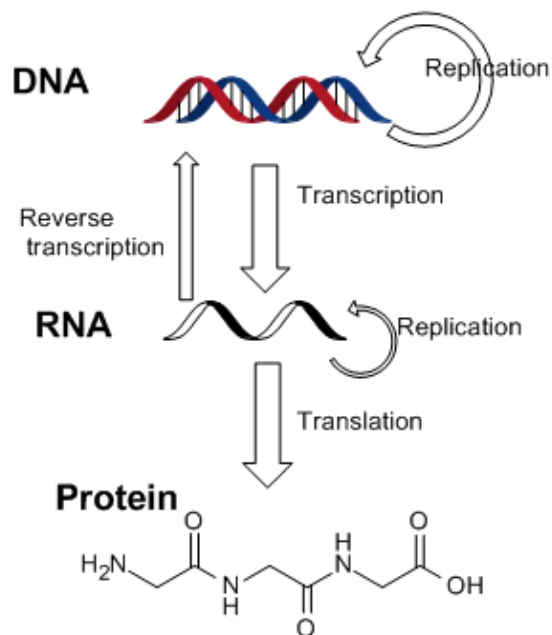


Figure 1.1: The flow of information in the central dogma of molecular biology.

At the start of the 21st century the human genome was completely sequenced [7-8]. The haploid human genome consists of three billion base pairs and only 25000 genes. This means that only 1.5% of the human genome contains heritable information. The rest of the DNA does not have any heritable information and most of it is non-coding DNA called "junk DNA". It is the need to draw maximum benefit from human genome project. Therefore many drugs have been synthesized which target DNA directly [9-10].

DNA is arranged in chromosomes inside cells and consist of up to millions of base pairs. The information in DNA is stored in the form of genes. Genes are specific regions of DNA that contain the heritable information, having characteristics like promotor sequences upstream and a stop codon downstream. Sets of three nucleotides that are translated into specific amino acids are called codons. For 20 amino acids, there are 64 codons ($4^3 = 64$), and since there are more codon combinations than amino acids, some amino acids have more than one codon. There are three stop codons (UAG, UAA and UGA) which terminate translation.

Nucleotides are the building blocks of DNA and consist of three components; a nitrogen base, a ribose sugar and a phosphoric acid (figure 1.2 a). The nitrogen bases are subdivided in two types; purines and pyrimidines. The purines in DNA are adenine (A) and guanine (G) while the pyrimidines are thymine (T) and cytosine (C) (figure 1.2 b). The base pairing in the DNA duplex is specific, A pairs with T while G pairs with C through two and three hydrogen bonds, respectively. The backbone of DNA is composed of alternating sugar and phosphate groups linked by phosphodiester bonds [11]. The phosphate groups give a negative charge to DNA. The hydrophobic nitrogen bases are on the inner side of DNA.

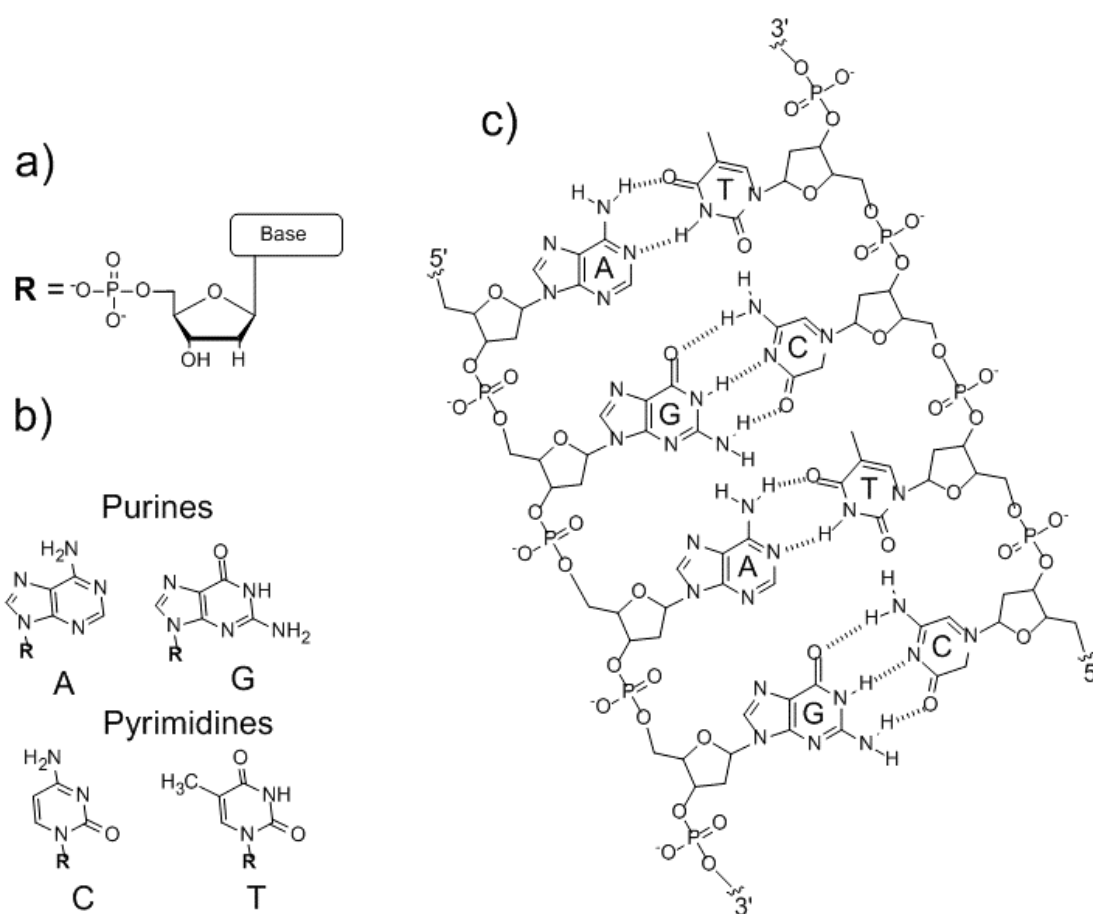


Figure 1.2: The structure of DNA; (a) A nucleotide containing a sugar, a phosphate, and a nitrogen base (b) The DNA bases, purines [adenine (A) and guanine (G)]and pyrimidines [thymine (T) and cytosine (C)] (c) The base pairing of DNA; A pairs with T and G pairs with C in an antiparallel fashion.

The DNA has a helical duplex structure in which DNA strands are complementary (anti-parallel) to each other (figure 1.2c). DNA has a helical duplex structure in which the DNA strands are complementary (anti-parallel) to each other (figure 1.2 c). DNA can have a number of different conformations. The three most common are A-DNA, B-DNA, and Z-DNA. Both A-DNA and B-DNA have a right-handed conformation but Z has a left handed conformation. B-DNA is shorter in diameter and longer in length compared to A-DNA while Z-DNA is thinner in diameter and longer in length than B-DNA and A-DNA. B-DNA is the most common confirmation in living cells. The B-DNA helix is 3.4 nm each turn and the distance between adjacent base pairs is 0.34 nm. Due to the helical structure of DNA grooves are formed along the DNA. They are called major (22 Å) and minor (12 Å) groove due to their size [12]. The larger space in the major groove allows binding of different substances, especially transcription proteins, to the DNA [13]. The non-B conformations of DNA are associated with different diseases [14]. DNA also has other confirmations, such as triplexes and quadruplexes, but they are uncommon [15].

1.2 Metal based drugs and potential of ruthenium based drugs

Cisplatin (figure 1.3) was the first metal based anticancer drug, discovered by Rosenberg in 1965 [16], that binds to DNA. Cisplatin is still used in compound therapy with other drugs to treat various cancers like testicular, ovarian, oropharyngeal, bronchogenic, cervical and bladder carcinomas, lymphoma, osteosarcoma, melanoma and neuroblastoma [17-18]. Cisplatin is currently used in intravenous (IV) infusions. Scientists are trying to enhance the efficiency of Cisplatin with reduced cytotoxic effects and strive to develop controlled release formulations. Cisplatin has the ability to bind to DNA and also to sulfur containing molecules like proteins and small peptides like glutathione (GSH) [19], but the major factor for the cisplatin toxicity is formation of DNA adducts. Cisplatin-DNA adducts block replication and transcription and cause apoptosis. Due to the toxic effect of Cisplatin, extensive research is carried out and literally thousands of new platinum compounds have been synthesized. Unfortunately, none of the new compounds could replace Cisplatin from the market. Carboplatin and oxaliplatin (figure 1.3) are among the few platinum compound based drugs that are available in the market today.

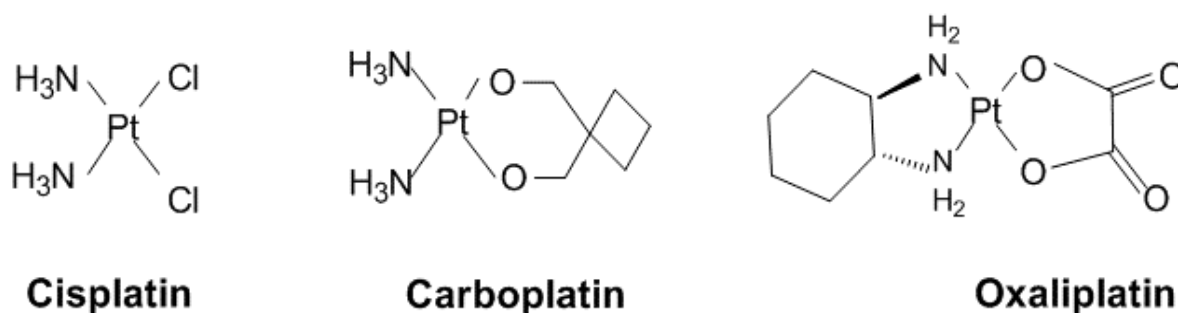


Figure 1.3: Chemical structure of different platinum based drugs available in the market.

The toxicity of platinum based drugs opens the gate for new metal based drugs with minimum or no side effects. Ruthenium is a potential candidate for such drugs and many ruthenium complexes intercalate DNA and slow down DNA replication. KP-1019 and NAMI-A are two ruthenium based drugs that bind to DNA and have passed phase I clinical trials [20-21]. Both drugs are ruthenium(III) complexes having octahedral geometry and four in-plane chloride ligands, one dimethylsulfoxid and one imidazole ligand in NAMI-A and two imidazole ligands in KP1019 (figure 1.4). The anti-cancerous activity of both complexes has been tested in different cell lines, in rodents and mouse. KP-1019 is taken up by cells efficiently and studies show that it untwists and bends DNA. Moreover KP-1019 is effective against solid tumors.

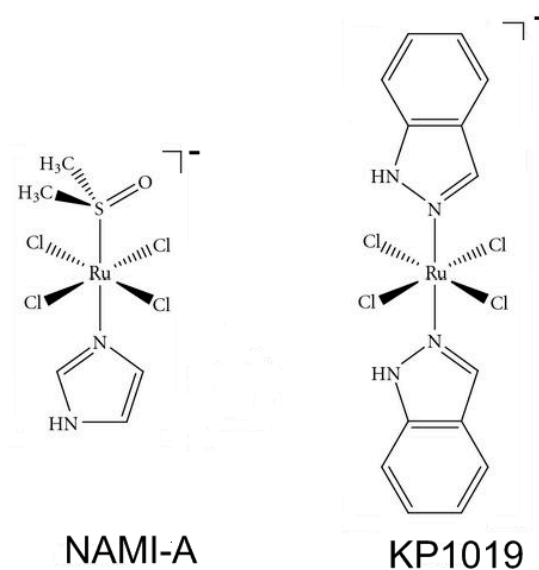


Figure 1.4: Chemical structure of ruthenium based drugs which are in clinical trial.

Ruthenium(III) drugs act as pro-drugs and are activated after reduction to ruthenium (II) by the “activation by reduction” mechanism [22]. The micro environment of cancer cells is different than the normal body environment because cancer cells grow very rapidly and have a high rate of glycolysis, producing lactic acid. Thus, the pH is lower in tumor cells which favors the reduction of ruthenium complexes. Moreover, ascorbic acid and glutathione can reduce ruthenium under normal physiological conditions. Ruthenium is transported in the blood by binding to albumin [23] and transferrin [24], both carriers for iron. Cancer cells divide very rapidly and require more iron and have more surface transferrin receptors than normal cells [25]. Since ruthenium is carried by transferrin, it can be transported to cancerous cells selectively. Thus, ruthenium based drugs do not harm healthy cells [22].

Recently the anti-bacterial activity of mononuclear ruthenium complexes $[\text{Ru}(\text{phen})_2\text{dpq}]^{2+}$, $[\text{Ru}(\text{bpy})_2\text{dpqC}]^{2+}$, and $[\text{Ru}(2,9\text{-Me}_2\text{phen})_2\text{dppz}]^{2+}$ was tested and complexes showed good antibacterial activity against gram positive bacteria like *B. subtilis*, *S. aureus* and also multidrug resistant bacteria such as methicillin-resistant *Staphylococcus aureus* (MRSA) but they showed less antibacterial activity against gram negative bacteria like *E.coli* [26]. The complex $[\text{Ru}(2,9\text{-Me}_2\text{phen})_2(\text{dppz})]^{2+}$ has

greater activity than the other two complexes. Moreover these complexes show no toxicity in *C. elegans*. Ruthenium complexes are also effective against protozoal diseases like malaria and trypanosomiasis [27]. Our work focuses on the pro-drug model of ruthenium complexes to achieve deep insight into the intercalation of ruthenium complexes with DNA in aqueous and hydrophobic crowded environments.

1.3 Ruthenium Polypyridyl Complexes

Ruthenium belongs to the transition metals and is situated below iron in the periodic table. Ruthenium has the ability to form various organometallic complexes in which ruthenium is the central atom surrounded by nitrogen containing ligands like 2,2'-bipyridine (bipy), 1,10-phenanthroline (phen) and dipyrido[3,2-a:2',3'-c] phenazine (dppz) (figure 1.5). Unlike Cisplatin which is a planar compound, ruthenium complexes have a octahedral geometry with left and right handed enantiomers.

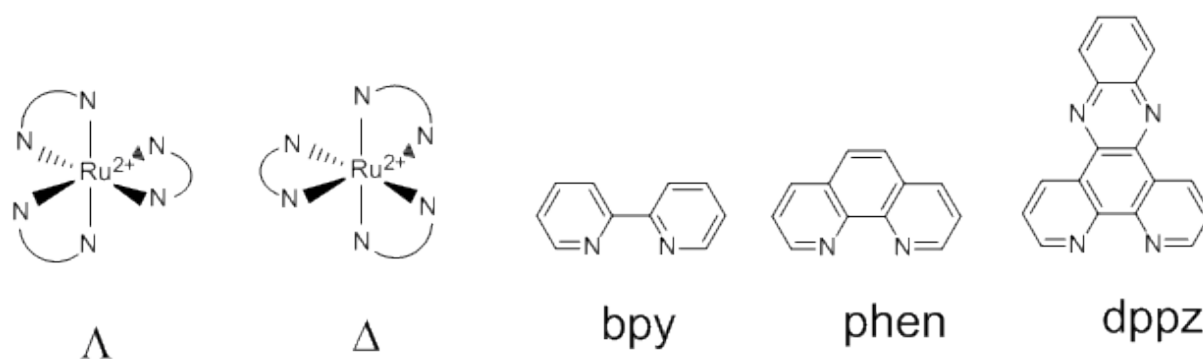


Figure 1.5: The left handed (Λ) and right handed (Δ) structures in which ruthenium is the central metal. The surrounding ligands bpy = 2,2'-bipyridine, phen = 1,10-phenanthroline and dppz = dipyrido [3,2-a:2',3'-c] phenazine (dppz).

Barton *et al* in 1984 reported intercalation of both the right handed (Δ) and the left handed (Λ) enantiomer of $[\text{Ru}(\text{phen})_3]^{2+}$ [28]. Since then ruthenium complexes are attractive candidates to study biomacromolecules because they are inert and bind to DNA non-covalently [29]. The photo-physical properties of the ruthenium complexes are enhanced by extending one phenanthroline to a dppz (dppz = dipyrido [3,2-a:2',3'-c] phenazine) to form the complex $[\text{Ru}(\text{phen})_2\text{dppz}]^{2+}$ (figure 1.6a). This complex intercalates into DNA by inserting its dppz part into base stack [30-31]. Both the Δ - and Λ -enantiomers binds to DNA stereo selectively, the Δ -enantiomer has a higher quantum yield than the Λ -enantiomer [30]. These complexes are fluorescent only when intercalated into DNA, where shielding of the dppz moiety from water results in a large increase in emission; the “molecular light switch effect” [31]. Thus a change in emission quantum yield is a useful property to study intercalation of these complexes. Mononuclear ruthenium complexes like $[\text{Ru}(\text{phen})_2\text{dppz}]^{2+}$ and $[\text{Ru}(\text{bipy})_2\text{dppz}]^{2+}$ (figure 1.6b) intercalate DNA rapidly.

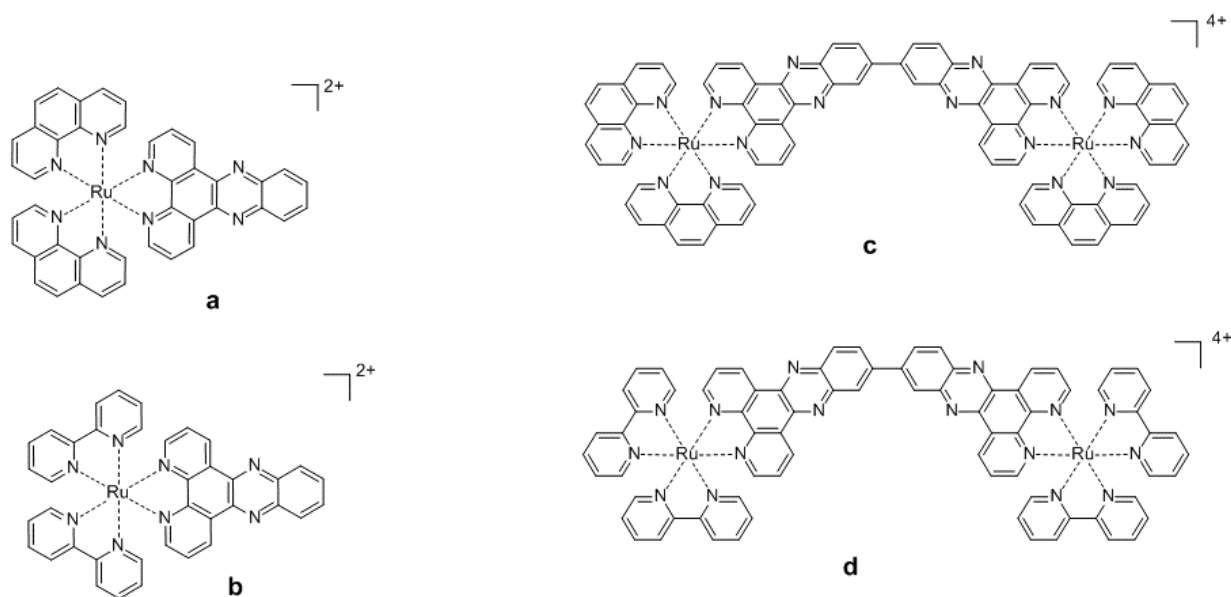


Figure 1.6: Structure of monomer: (a) $[\text{Ru}(\text{phen})_2\text{dppz}]^{2+}$, (b) $[\text{Ru}(\text{bipy})_2\text{dppz}]^{2+}$ and dimer ruthenium complexes: (c) $[\text{Ru}_2(\text{phen})_4\text{bidppz}]^{4+}$, (d) $[\text{Ru}_2(\text{bipy})_4\text{bidppz}]^{4+}$.

Binuclear ruthenium complexes were synthesized by connecting two monomers by a flexible [32], semirigid [33] or rigid [34] linker. Semirigid binuclear ruthenium complex with general formula $[\mu\text{-(dppz)}_2\text{L}_4\text{Ru}_2]^{4+}$ [where L=2,2'-bipyridine(B) and L= 1,10-phenanthroline (P)] (figure 1.6c-d) have been extensively studied due to their DNA threading property [33-34]. Early it was considered that they bind in the grooves of DNA [35], but later studies showed that they intercalate via threading into the duplex DNA [33]. Mechanical manipulation of one binuclear ruthenium complex ($\Delta\Delta\text{-P}$) threading into DNA with optical tweezers revealed that threading requires the opening of at least one base pair [36]. Threading of the complex is a two-step process. The first step is fast as it is based on electrostatic interaction between the negatively charged DNA and the positively charged ruthenium complex. The second step is slow and is the true threading step where one bulky group of the complex has to pass through the base stack of the duplex DNA (figure 1.7).

The binuclear ruthenium complexes thread DNA in a highly efficient way but the rate of association and dissociation is very slow [37]. The threading intercalation of binuclear complex is strongly dependent upon temperature. It is slow and takes days at room temperature but at 50°C threading will occur in approximately one hour [33]. Moreover the threading rate does not only depend on the structure of the complex but also on the sequence of the DNA [38-39]. Kinetic recognition of AT rich sequences has been reported in the literature, where these complexes thread into poly(AT) DNA up to 2500 times faster compared to mixed sequence calf thymus DNA [38]. Nordell *et al* investigated threading into a HEG-linked hairpin oligonucleotides with a central AT track of 6 to 44 base-pairs [40]. The threading rate for the of nucleotide with 10 AT repeats resembled ct-DNA while increasing the number of AT repeats to 14 the threading rate was higher and resembled poly (AT) DNA much more. This finding revealed that the length of the AT track is an important factor to determine the

DNA threading rate. The malarial parasite *Plasmodium falciparum* genome has about 80% AT base pairs [41]. Since these complexes selectively bind to AT rich DNA instead of mixed sequence DNA, they might be used as antimalarial agents [38-39]. All these findings illustrate that ruthenium complexes have great potential for the development of therapeutics.

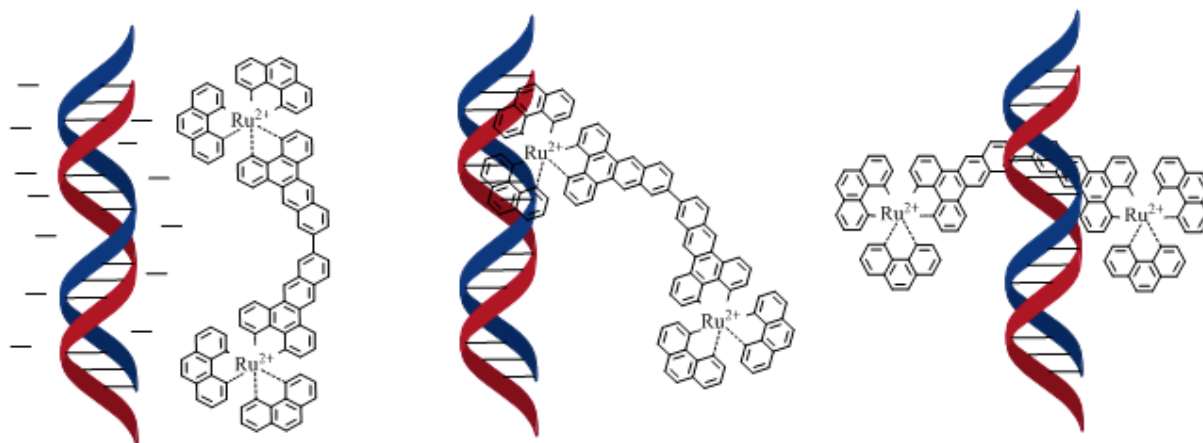


Figure 1.7: Schematic representation of the threading of complex P into DNA. First the positively charged complex electrostatically attracts to DNA (left), coordinates with one of the DNA base (middle) and finally thread into the DNA (right).

Just like the monomers, the binuclear complexes show the lightswitch effect when threaded into DNA. Thus an increase in luminescence is related to the association kinetics and a decrease in luminescence is linked to dissociation of the complex from DNA. Sodium dodecyl sulfate (SDS), an anionic surfactant, catalyzes the dissociation of cationic metal complexes from DNA [37, 42-43]. The SDS monomers accumulate around the positively charged DNA-bound metal complex and lower the energy barrier for dissociation. SDS has different catalytic effect on the dissociation for P and B and the less hydrophobic B complex is associated with a higher catalytic effect than the more hydrophobic complex P [37].

1.4 Molecular Crowding

Cells contain biomacromolecules such as proteins, lipids, nucleic acids and polysaccharides that collectively with other molecules comprise about 30-40% of the cellular volume, creating a crowded environment inside the cell (figure 1.8) [44-46]. Cellular reactions occur in a crowded environment *in vivo*, but most biological reactions studied *in vitro* are not in a crowded environment [47-48] and therefore do not represent the exact scenario *in vivo* [49]. Intracellular crowding results in self assembly of macromolecules like densely packed DNA, packaging of polypeptides to form functional proteins and packaging of other polymers. Many vital biological reactions like DNA-DNA interactions, DNA-protein interactions and protein-protein interactions are supported by molecular crowding [50-54].

A variety of molecules like dextran, polyethylene glycol (PEG) and Ficoll are used as crowding agent to mimic the intracellular crowding *in vitro*. The crowding agent must be inert, properly dissolved in

water and not interfere with the target molecule. Dextran is a polymer of glucose molecules, PEG is polymer of ethylene glycol (figure 1.8) and Ficoll is a copolymer of sucrose and epichlorohydrin. Some proteins like albumin and hemoglobin can also be used as crowding cosolutes [46].

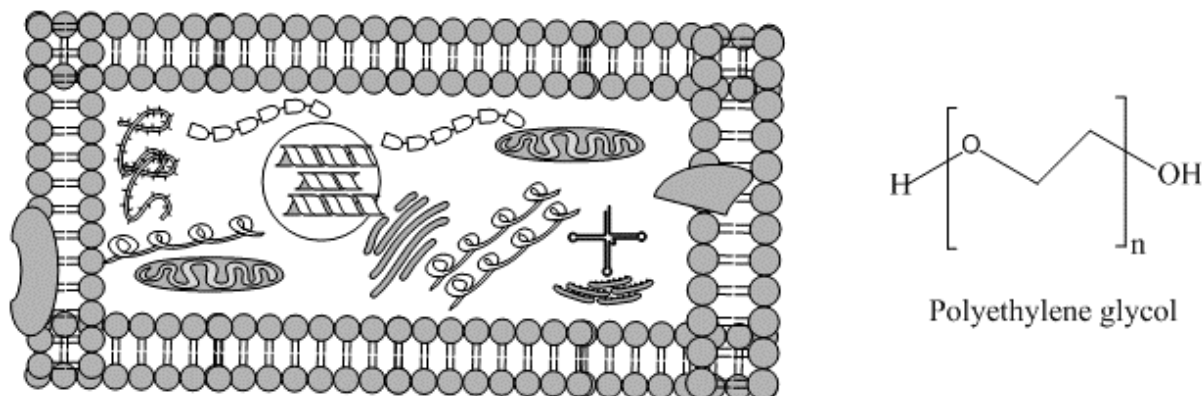


Figure 1.8: The macromolecular crowding inside the cell due to the presence of biomacromolecules (left) and the structure of polyethylene glycol (right).

The effect of molecular crowding on structure and stability of nucleic acids both *in vivo* and *in vitro* is presently of great interest [47, 55]. The stability and structure of DNA in a crowded environment depends on the number of nucleotides in DNA, the size and the concentration of cosolutes. PEG affects the stability of nucleic acids, the concentration of PEG is important in regards of both entropy and enthalpy of the DNA duplex. Higher concentrations of PEG destabilize the DNA duplex by affecting the water activity inside the DNA duplex. Long and short duplexes behave differently in a crowded environment [56]. Long DNA duplex is linked with compaction and condensation under the influence of crowding. Short DNA duplexes are less affected by crowding agents. Therefore short oligonucleotides are suitable for quantitative studies in presence of crowding agents. Oligonucleotides (8-30-mers) maintain Watson-Crick base pairing in the presence of a crowding agent such as PEG in aqueous solution [57-58].

Recently Feng *et al* reported that PEG catalyzes DNA strand exchange [58]. From this study, it is not clear if the catalytic activity of PEG is due to a decrease in water activity or molecular crowding. The present study gives insight into the catalytic activity of PEG. The crowding is not expected to have any effect on threading because the initial interaction between the complex and DNA is electrostatic and thus not affected by crowding. Changes in the water activity can affect the duplex conformation of DNA and it might be possible that hydrophobic interactions between DNA and PEG will result in destabilization of the DNA duplex. If PEG catalyzes the threading that means that water activity is important in regards of the catalytic activity of PEG.

1.5 Objectives of our work

The goal of our work is to study the effect of molecular crowding, induced by PEG, on the threading rate of ruthenium complexes with various DNA models. We use three DNA model systems in our study, mixed sequences calf thymus DNA (ct-DNA), sonicated ct-DNA and a short synthetic oligonucleotide with a HEG-linked hairpin.

Due to the condensation of ct-DNA and sonicated ct-DNA in presence of high concentrations of PEG we could not draw any solid conclusion from their results. 10% PEG catalyzes the DNA threading for both P and B complexes. The results for the synthetic oligonucleotide are more promising and support our hypothesis that threading rate is increased in PEG crowded environment. We observed that the threading is more sensitive to PEG at lower concentrations compared with DNA strand exchange. 40% PEG has very little catalytic effect on strand exchange but in our study there is a significantly higher threading rate in 40% PEG compared to in buffer.

2. Fundamental concepts

2.1 UV-visible Spectroscopy

When light of a certain wavelength passes through a solution some light is absorbed and the rest is transmitted. The fraction of absorbed light is described by the Beer–Lambert law:

$$A(\lambda) = \epsilon(\lambda) c l$$

where absorbance, A , is directly proportional to the concentration (c) and path length (l), ϵ is the extinction coefficient and λ is the wavelength.

Spectroscopy is a technique used to determine the concentration of a given chemical species. A spectrophotometer consists of a light source, a monochromator (used to select wavelength), a sample holder (cuvette) and a detector (detects change in the intensity of incident and transmitted light) (figure 2.1).

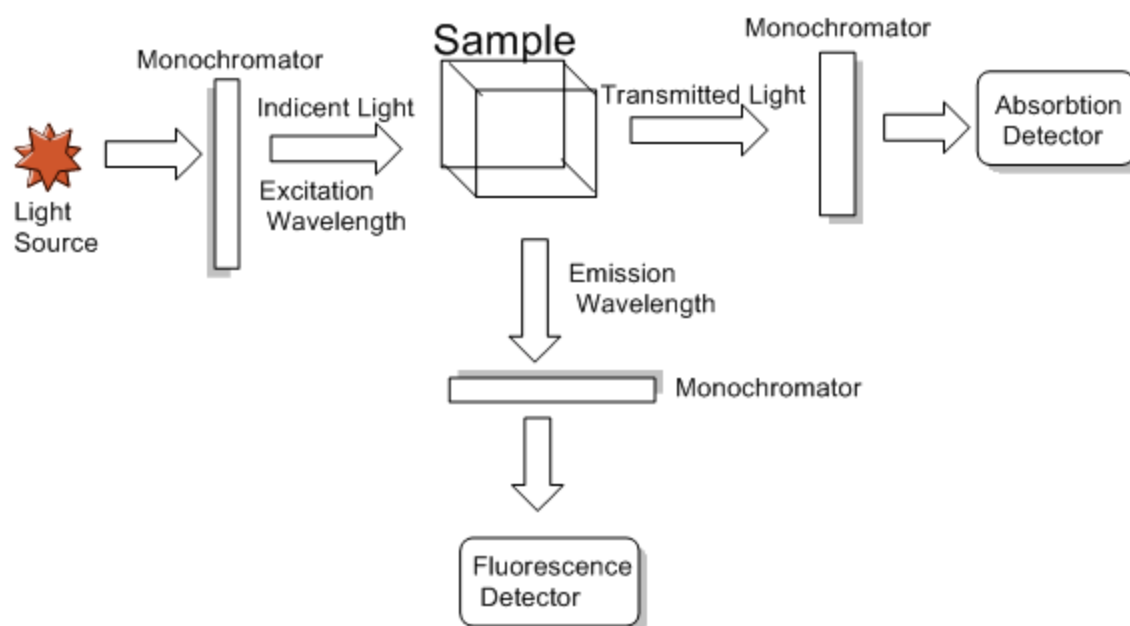


Figure 2.1: Schematic representation of absorption and fluoresce spectroscopy.

2.2 Fluorescence Spectroscopy

The Jablonski diagram was proposed by Alexander Jablonski in 1935 and shows a schematic representation of absorption and emission after electronic excitation in a molecule. The different states of the electron, ground state (S_0), first (S_1) and second (S_2) excited state are shown in figure 2.2 and every state has several vibrational levels. If a photon with energy ($h\nu_A$) is absorbed by a molecule, a ground state electron is excited to a higher energy level (S_2 or S_1).

After excitation the excited electron relaxes to the lowest energy level (S_1) via vibrational relaxation. When the molecule is relaxed, the electron can return to the ground state by emitting the energy in the form of fluorescence ($h\nu_F$) or by non-radiative processes. In certain cases the electron first goes to the triplet excited state (T_1) and where the relaxation energy can be released in the form of phosphorescence ($h\nu_P$).

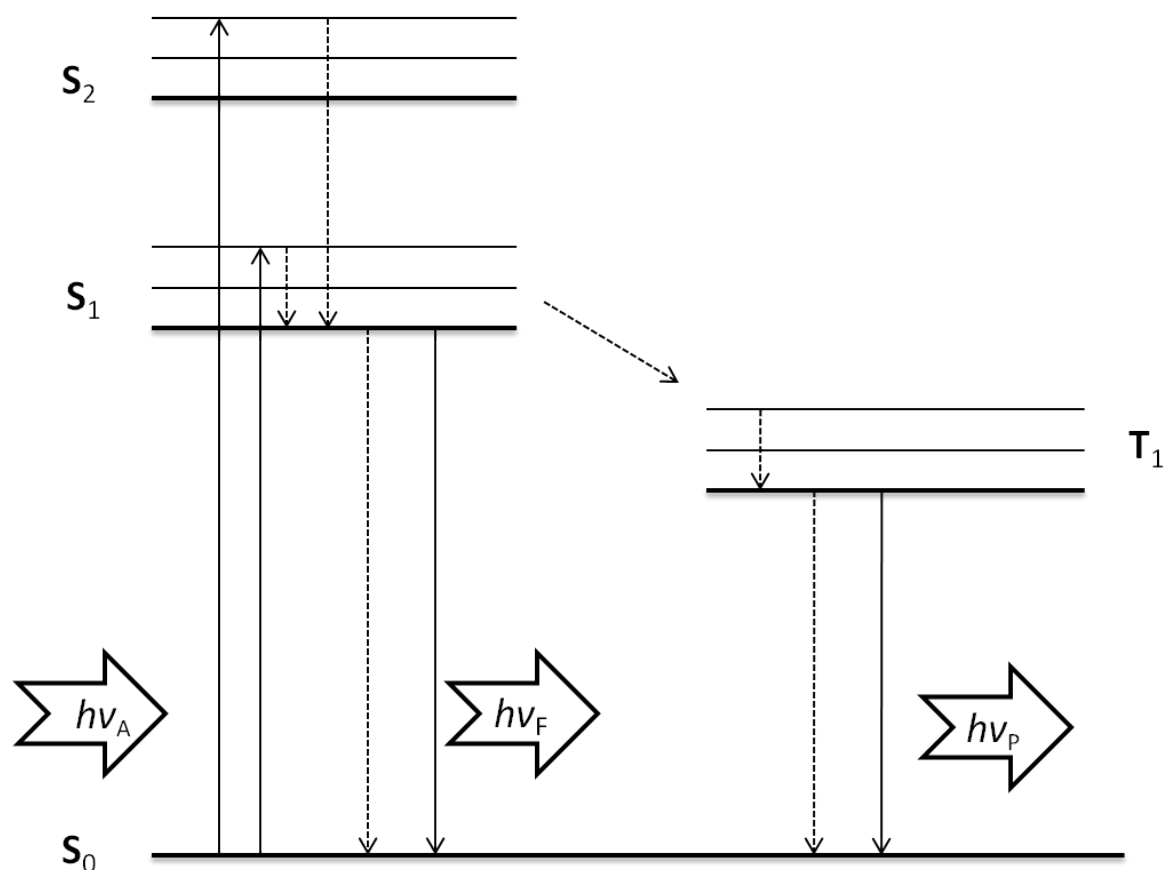


Figure 2.2: The Jablonski diagram. Solid lines represent the radiative process such as fluorescence ($h\nu_F$) and phosphorescence ($h\nu_P$) and dashed lines represent non-radiative processes. S_1 , S_2 and T_1 are excited states and S_0 is the ground state.

Fluorescence spectroscopy is used to measure the fluorescence of various fluorescent compounds. High energy photons are used to excite the sample which in turn emits photons of a lower energy. We can measure emission spectra (emission at different wavelengths at constant excitation wavelength) and excitation spectra (excitation at different wavelength at constant emission wavelength) using fluorimeters (figure 2.1).

We employed fluorescence emission spectroscopy in our study to investigate the binding kinetics of the ruthenium complexes. The ruthenium complexes are not fluorescent when bound to the outside of the DNA but fluoresce strongly when intercalated. Therefore an increase in the emission of our sample is proportional to the degree of intercalation.

2.4 Linear dichroism (LD)

Linear dichroism (LD) is a spectroscopic technique used to study the structure of biomacromolecules like DNA. Plane polarized light is used to interact with the sample and absorbance is taken in parallel and perpendicular to molecules like DNA. Larger molecules like DNA can be oriented by applying an electric or magnetic field or by a flow gradient. We use flow LD to align DNA in this study. The sample containing DNA is placed, in a specially designed Couette cell (figure 2.3), between the walls of two quartz cylinders (the gap between the two cylinders is approximately 0.5 mm, thus the path length is 1 mm). DNA is oriented perpendicular to the axis of rotation by rotating one of the two cylinders. LD can be calculated as the difference in absorbance of light linearly polarized parallel (A_{\parallel}) and perpendicular (A_{\perp}) to the axis of orientation.

$$LD = A_{\parallel} - A_{\perp}$$

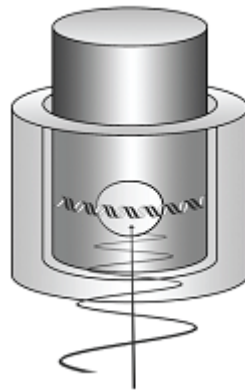


Figure 2.3: The LD Couette cell. Long polymers like DNA are aligned along the direction of the flow produced by rotation one of the two cylinders.

Small molecules that bind to DNA will cause a change in the LD signal. If a planar molecule binds DNA parallel to the plane of the bases ($\alpha \approx 90^\circ$) this gives a negative LD signal, but if the molecule binds the DNA in an orientation that is parallel to the DNA grooves ($\alpha \approx 45^\circ$) a positive LD signal is generated.

3. Materials and Methods

3.1 PEG and Buffer

Polyethelene glycole (PEG), used to produce a crowded environment. PEG-6000 (Sigma) was obtained as white flakes with heterogeneous degrees of polymerization and an average molecular weight at 6000 g/mol. PEG flakes are dissolved in buffer to produce a solution of 10-50% PEG (weight/weight solution). 150 mM NaCl (1mM cacodylate, pH = 7) solution was used as aqueous buffer and denoted as “buffer” in the rest of the thesis.

3.2 Ruthenium complexes

The monomer (Δ -P and Λ -B) and binuclear ($\Delta\Delta$ -P and $\Lambda\Lambda$ -B) ruthenium complexes used in this study (figure 1.7), were synthesized as described elsewhere [30, 59-60] and kindly provided by Johnna Andersson and Per Lincoln. The ruthenium complexes are dissolved in PEG solutions and buffer. The concentration of these complexes is measured with a spectrophotometer using baseline correction. The extinction coefficient for both monomers is $\epsilon_{440} = 20000 \text{ cm}^{-1}\text{M}^{-1}$ and the extinction coefficients for the binuclear complexes are $\Delta\Delta$ -P : $\epsilon_{410} = 75800 \text{ cm}^{-1}\text{M}^{-1}$ and $\Lambda\Lambda$ -B : $\epsilon_{410} = 65000 \text{ cm}^{-1}\text{M}^{-1}$ respectively.

3.3 DNA models

We used three different DNA model systems; calf thymus DNA (ct-DNA), sonicated ct-DNA and a synthetic oligonucleotide with a central AT track called TA6. Highly polymerized type I sodium calf thymus DNA was purchased from Sigma–Aldrich. Lyophilized ct-DNA was dissolved in aqueous buffer and filtered three times through a 0.8 μm Millipore filter before use. The concentration of the nucleotide bases was determined at 260 nm using extinction coefficient $\epsilon_{260} = 6600 \text{ cm}^{-1}\text{M}^{-1}$. TA6, was purchased from atdBio, is a hexaethylene glycol (HEG) linked hairpin and the sequence is 5'-CCGGXGGCC-HEG-GGCCXCCGG-3' where X = 12 AT base pairs. The concentration of TA6 is calculated using $\epsilon_{260} = 363600 \text{ cm}^{-1}\text{M}^{-1}$.

3.4 Experimental setup

The concentration used in the experiments is 50 μM nucleobases for ct-DNA and 1.56 μM ruthenium complexes (base pair to complex ratio = 1:16). The ct-DNA was sonicated to reduce the strand length from about 10,000 bps to 200-400 bps. The ratio of sonicated nucleobases to complex was 5 base-pairs per one complex. Concentration of TA6 and ruthenium complexes used in the experiments was 0.25 μM each (duplex strand of TA6 to complex ratio was 1:1).

Both DNA and ruthenium complex were mixed in buffer and PEG were pre-incubated at the temperature at which the kinetics was measured. The DNA is added at the start of the experiment, vortexed to

mix properly and then centrifuged for a few seconds to remove air bubbles and transferred to the cuvette, and then the kinetics was measured. Kinetic traces were taken at excitation wavelength 410 nm and emission was recorded at 625 nm. The emission and excitation slits are 5 nm for $\Delta\Delta$ -P and 10 nm for $\Delta\Delta$ -B in all experiments for ct-DNA while for TA6 the emission and excitation slits are 10 nm for $\Delta\Delta$ -P.

3.5 Instrumentation

Concentration of DNA and ruthenium complexes was measured using a Varian Cary 5000 UV-Vis or a Cary 50 Bio UV-Vis spectrophotometer in a quartz absorption cuvette. Fluorescence emission kinetics was measured using a Varian Cary Eclipse spectrofluorimeter, equipped with a multicell temperature controller. The Flow LD was measured using a Jasco J-720 equipped with an oxley prism to get linearly polarized light. The flow Couette cell (figure 2.3) has an outer rotating shell and an inner fixed quartz filler with a path length of 1 mm (0.5 mm on both sides) and the measurements were taken at 1000 rpm and corrected for baseline (measured with out rotation).

3.6 Data Analysis

Data was analyzed using Origin version 6, by Microcal Software USA.

4. Results and Discussion

The results and discussion on the effect of PEG on the rate of threading in different model systems are presented in this chapter. First we present the threading kinetics of dimer ruthenium complexes into ct-DNA, followed by flow LD of both dimer ($\Delta\Delta$ -P and $\Lambda\Lambda$ -B) and monomer (Δ -P and Λ -B) complexes bound to DNA in different PEG concentrations and in buffer. Finally, the results for the threading into a short oligonucleotide are presented.

4.1 Calf thymus DNA and $\Delta\Delta$ -P

The threading kinetics was measured at different PEG concentrations at various temperatures. The threading intercalation of binuclear ruthenium complexes with DNA results in a rapid increase in emission quantum yield due to the light-switch effect and the threading rate can therefore be conveniently studied.

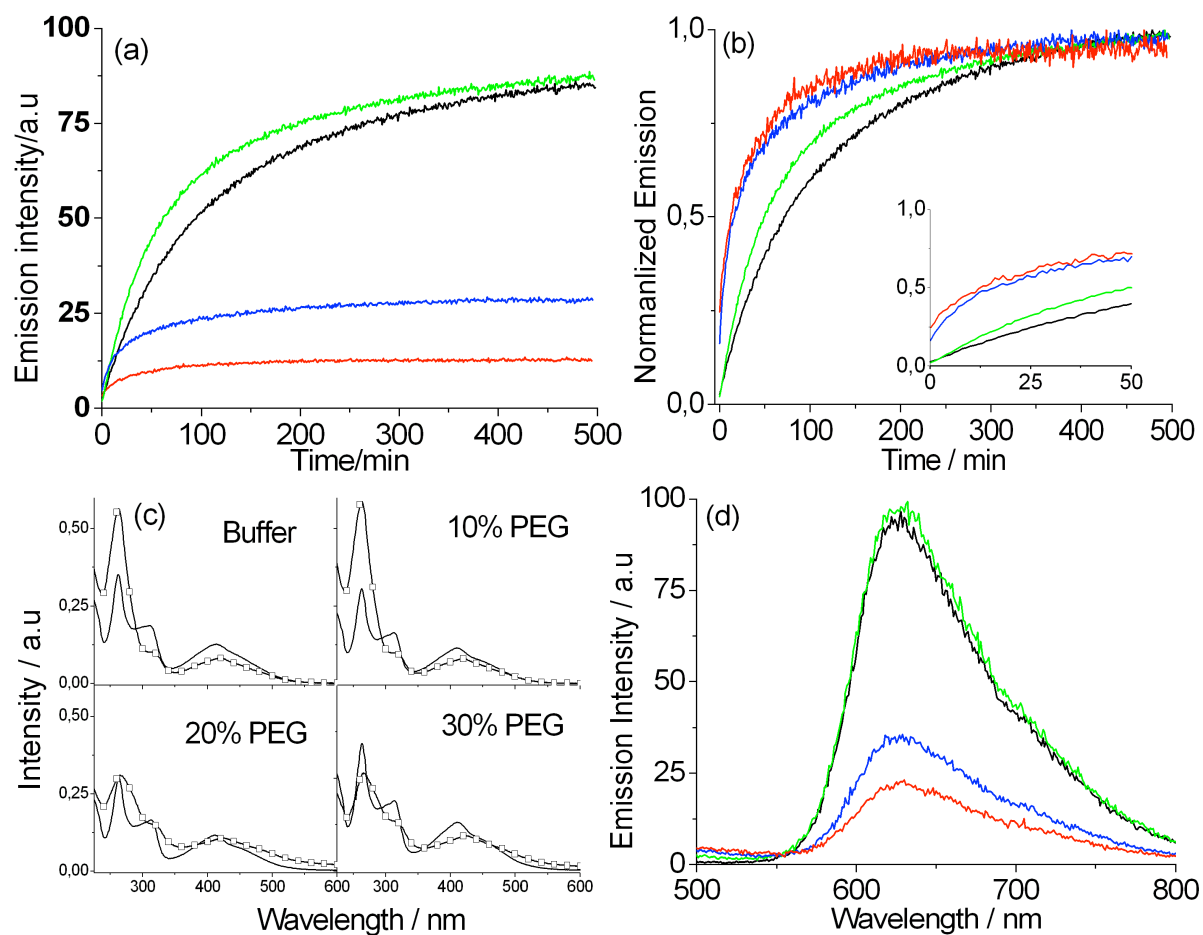


Figure 4.1: Threading kinetics for $\Delta\Delta$ -P into ct-DNA at 45°C (a) kinetic traces (b) normalized kinetic traces (normalized after 500 minutes) and inset: initial phase (c) absorption spectra before = --- and after adding DNA = -□- (d) steady state emission spectra in different PEG concentrations (10% PEG = green, 20% PEG = blue and 30% PEG = red) and buffer = black. Both absorption and emission spectra are taken at room temperature.

Figure 4.1a shows the change in emission intensity of $\Delta\Delta$ -P with time after addition of ct-DNA at 45°C in PEG and in buffer. The emission is higher in 10% PEG and buffer compared to 20 and 30% PEG. In 10% PEG the emission increases faster than in buffer but with time the emission intensities becomes similar. To compare the rates, the kinetic traces were normalized (figure 4.1b). The rate in 20 and 30% PEG is almost similar and faster than in buffer and 10% PEG. We were surprised to see that the emission is lower at higher PEG concentrations. Thus we measured absorption spectra (figure 4.1c) after the kinetics. The absorption spectra in buffer and 10% PEG are similar with literature indicating that the complex is intercalated into DNA [61-62]. The DNA peak in 20 and 30% PEG is much smaller compared to in buffer and in 10% PEG and light scattering at long wavelengths indicates aggregation and precipitation of DNA. Thus it is hard to draw any conclusion from the kinetic measurements. The steady state emission spectra (figure 4.1d) after 1000 minutes shows similar trend as figure 4.1a indicating that nothing happens after 500 minutes.

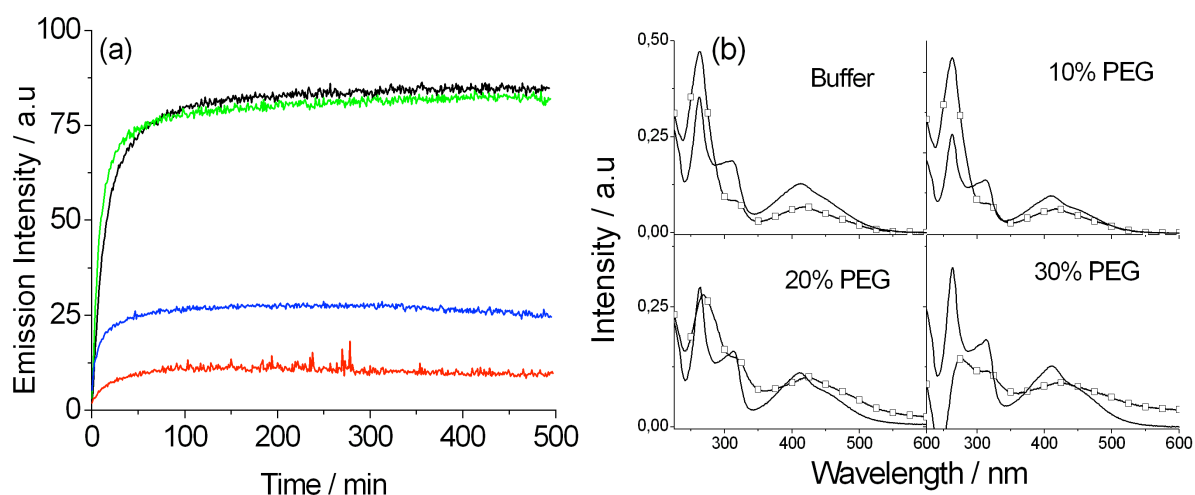


Figure 4.2: Threading kinetics for $\Delta\Delta$ -P into ct-DNA at 55°C (a) kinetic traces at different PEG concentrations (10% PEG = green, 20% PEG = blue and 30% PEG = red) and Buffer = black (b) Absorption spectra before = --- and after adding DNA = -□-. Absorption spectra are taken at room temperature.

Figure 4.2a shows the kinetics at 55°C in buffer and in different PEG concentrations. The trend is similar to 45°C but the signal is noisier at high PEG concentrations. The signal is noisy at high PEG concentrations, which indicates even more aggregation at this temperature. To investigate the aggregation, absorption spectra (figure 4.2b) were measured. The absorption spectra were similar to 45°C but with more aggregation at 55°C. The DNA peak in higher PEG concentrations is much smaller and they also scatter light at higher wavelengths due to aggregates of DNA. Therefore the decrease in emission intensity in 20 and 30% PEG is due to aggregation / precipitation of DNA. The precipitation of DNA-bound complex is a problem for this complex and we can not draw any solid conclusion from these results.

4.2 Calf thymus DNA and $\Lambda\Lambda$ -B

In order to study the effect of the ancillary ligands of the ruthenium complex on DNA threading rate in PEG, the less hydrophobic complex (B) was investigated. $\Lambda\Lambda$ -B and $\Delta\Delta$ -P behave similarly in buffer but the emission is lower for $\Lambda\Lambda$ -B [62]

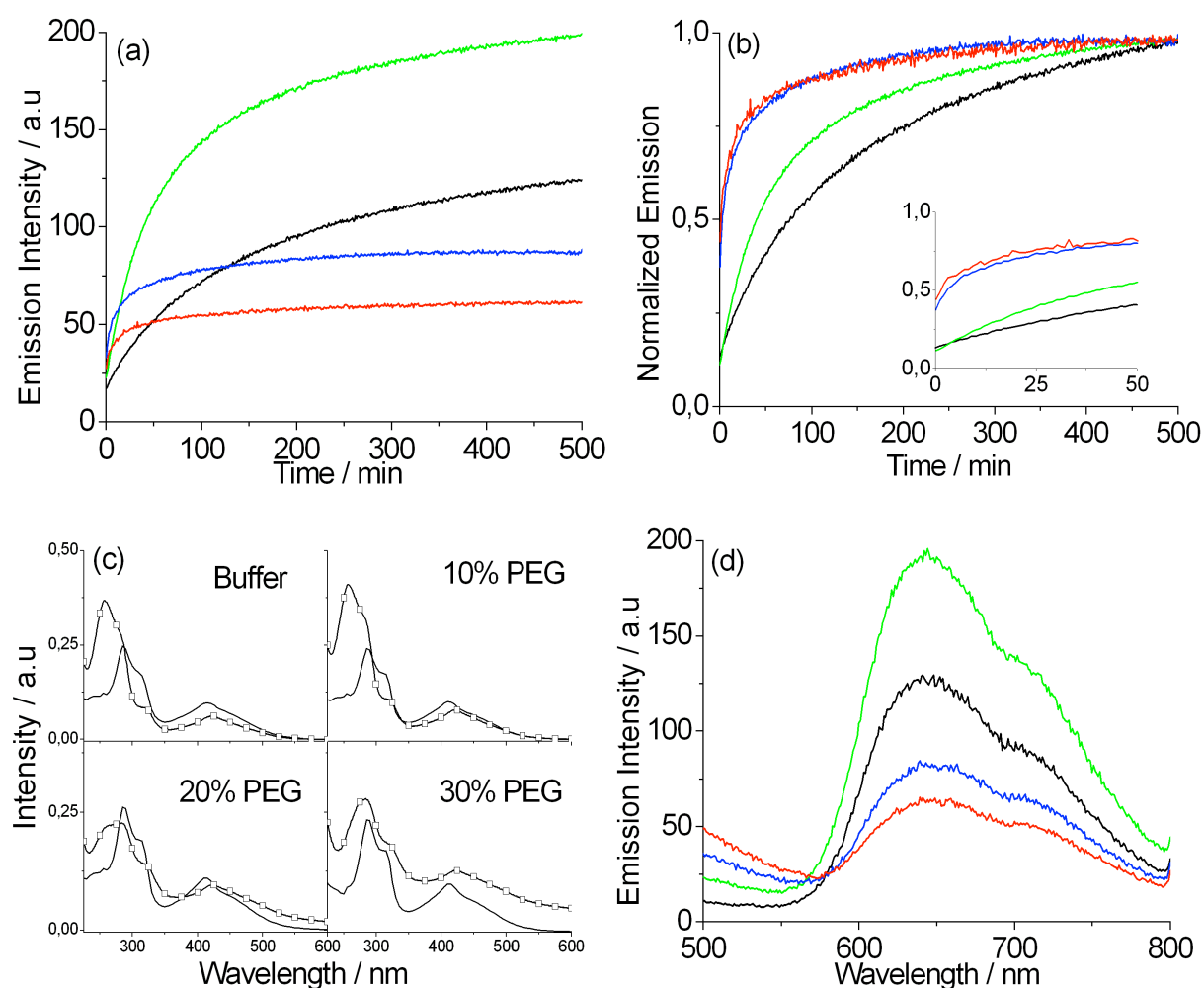


Figure 4.3: Threading kinetics for $\Lambda\Lambda$ -B into ct-DNA at 45°C (a) kinetic traces (b) normalized kinetic traces (normalized at 500 minutes) and inset: initial phase (c) absorption spectra before (---) and after adding DNA (-□-). (d) Steady state emission spectra in different PEG concentrations (10% PEG = green, 20% PEG = blue and 30% PEG = red) and buffer = black. Both absorption and emission spectra are taken at room temperature.

Figure 4.3a shows the change in emission quantum yield with time for $\Lambda\Lambda$ -B after addition of ct-DNA at 45°C. The emission intensity is highest in 10% PEG and lowest in 30% PEG. There is a significant difference in emission intensity in buffer and in 10% PEG not detected for complex P at the same temperature. The kinetic traces are normalized (figure 4.3b) to compare the rates. The threading rate is similar in 20 and 30% PEG and higher than in buffer and 10% PEG. To investigate why the emission is lower at high PEG concentrations, we again measured absorption spectra (figure 4.3c) after kinetics. The absorption spectra were similar to $\Delta\Delta$ -P in buffer and 10% PEG. Light scattering was observed at higher wavelengths in 20 and 30% PEG due to aggregation of DNA. The DNA peak is also much

lower in high PEG concentrations compared to in buffer and 10% PEG. Thus it is hard to say anything about the kinetics for B due to aggregation of DNA just like for complex P. The steady state emission spectra after 1000 minutes are similar to the kinetics and thus nothing changes after 500 minutes.

Figure 4.4a shows the threading kinetics at 55°C. At this temperature the rate is higher in buffer and PEG as predicted. High PEG concentrations again have lower emission and absorption spectra show that the band at 260 nm in 20 and 30% PEG is low and light scattering is more prominent at this temperature compared to 45°C. A slight aggregation was detected also in 10% PEG at this temperature. Thus more aggregation and light scattering is observed at 55°C compared to 45°C for both P and B complexes.

To summarize the results for ct-DNA, 10% PEG catalyzes the DNA threading and higher PEG concentrations (20-30% PEG) cause aggregation / precipitation of ct-DNA especially at high temperatures. Therefore the results of high PEG concentrations are not reliable.

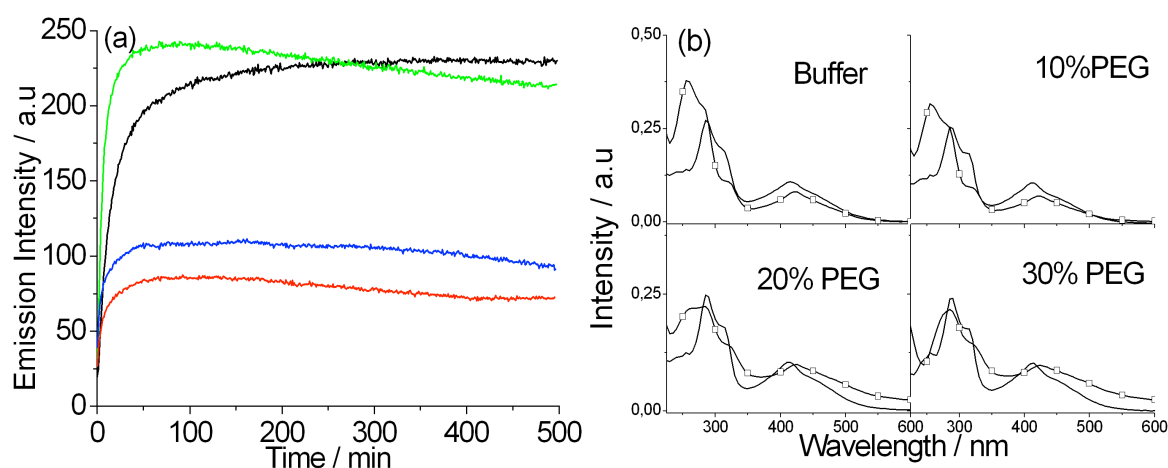


Figure 4.4: Threading kinetics for $\Lambda\Lambda$ -B into ct-DNA at 55°C (a) kinetic traces at different PEG concentrations (10% PEG = green, 20% PEG = blue and 30%PEG = red) and buffer = black. (b) Absorption spectra before (---) and after (-□-).The absorption spectra are taken at room temperature.

4.3 Linear dichroism of monomer and dimer complexes with ct-DNA

Linear dichroism (LD) is an effective tool to measure the binding geometry of ligands with biomacromolecules like DNA. We use flow LD to align ct-DNA and study whether the complex is intercalated or not and to determine the degree of condensation and compaction of DNA in PEG. The change in LD at 320 nm is due to the binding geometry of the dppz ligand and a variation at 260 nm represents a change in DNA orientation. Condensation of DNA leads to a reduced LD signal, because the condensed DNA is not properly aligned by the flow.

The parent monomers of these complexes also intercalate into DNA [63]. We use the monomers to investigate if they behave similar to the dimers in PEG. LD spectra (figure 4.5) in buffer and 10%

PEG show a negative LD signal from DNA and also a negative signal from $\Delta\Delta$ -P (figure 4.5a) showing that it is intercalated. The LD signal is higher in 10% PEG compared to in buffer at 260 nm. In higher PEG concentrations (15-30%), no LD signal from DNA was detected for this complex indicating DNA condensation. $\Delta\Delta$ -B (figure 4.5b) has a similar trend as P but the LD signal is almost similar for buffer and 10% PEG. The monomer Δ -P (figure 4.5c) also shows intercalation with DNA in buffer but in 20 and 30% PEG no LD signal was detected due to aggregation. For Δ -B (figure 4.5d) the DNA signal starts to decrease in 15% PEG but the monomer signal can be detected while the dimer did not show any LD at this temperature. Therefore we suggest that the monomers are less aggressive than dimers. The monomers contains one while the dimer contain two ruthenium centers and they have 2 and 4 positive charges, respectively. Therefore the charge of the intercalating molecule is important in regards of DNA condensation in a crowding environment.

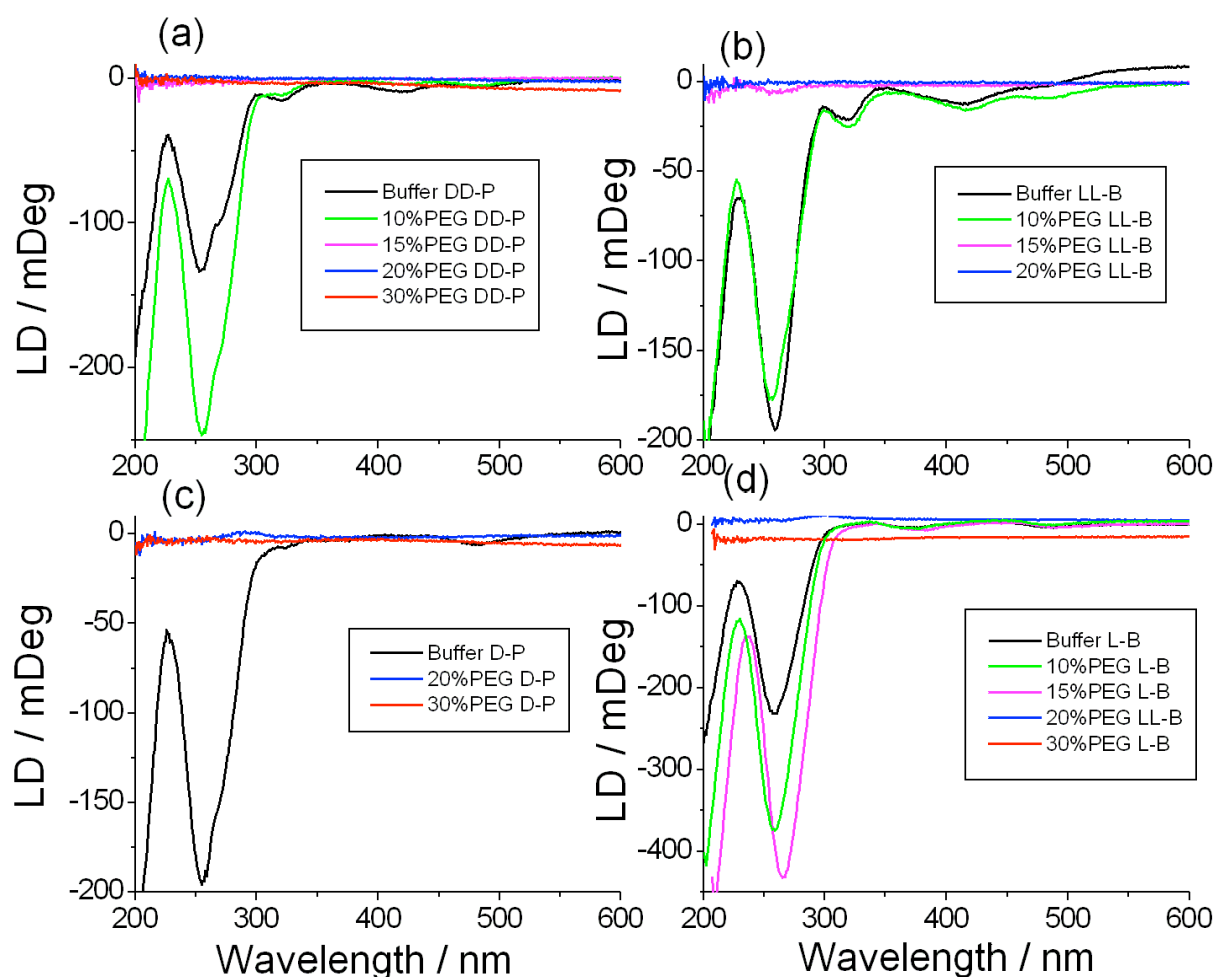


Figure 4.5: Linear dichroism spectra for $\Delta\Delta$ -P (a), $\Delta\Delta$ -B (b), Δ -P (c) and Δ -B (d) in different PEG concentrations and in buffer after overnight incubation at 50°C. The measurements are taken at room temperature. Note the different Y-axis scales.

4.4 Temperature dependent threading rate in buffer and 10% PEG for ct-DNA

Ct-DNA aggregates in the presence of ruthenium dimers at higher PEG concentrations whereas 10% PEG shows no or very slight aggregation, thus we compare the rates in buffer and 10% PEG. The threading rate is higher in 10% PEG compared to in buffer for both $\Delta\Delta$ -P and $\Lambda\Lambda$ -B into ct-DNA at all temperatures (figure 4.6). There is larger difference in rate at higher temperatures. PEG seems to have less catalytic effect for complex $\Delta\Delta$ -P compared to $\Lambda\Lambda$ -B. Westerlund *et al.*, reported that SDS catalyzes the dissociation of binuclear ruthenium complexes by lowering the energy of activation for dissociation. They also report that SDS has a higher catalytic effect for $\Lambda\Lambda$ -B compared to $\Delta\Delta$ -P [37]. Our results show that the hydrophobic interactions are not only important for dissociation of complex from DNA but also for the association and the effect is smaller for $\Delta\Delta$ -P than $\Lambda\Lambda$ -B.

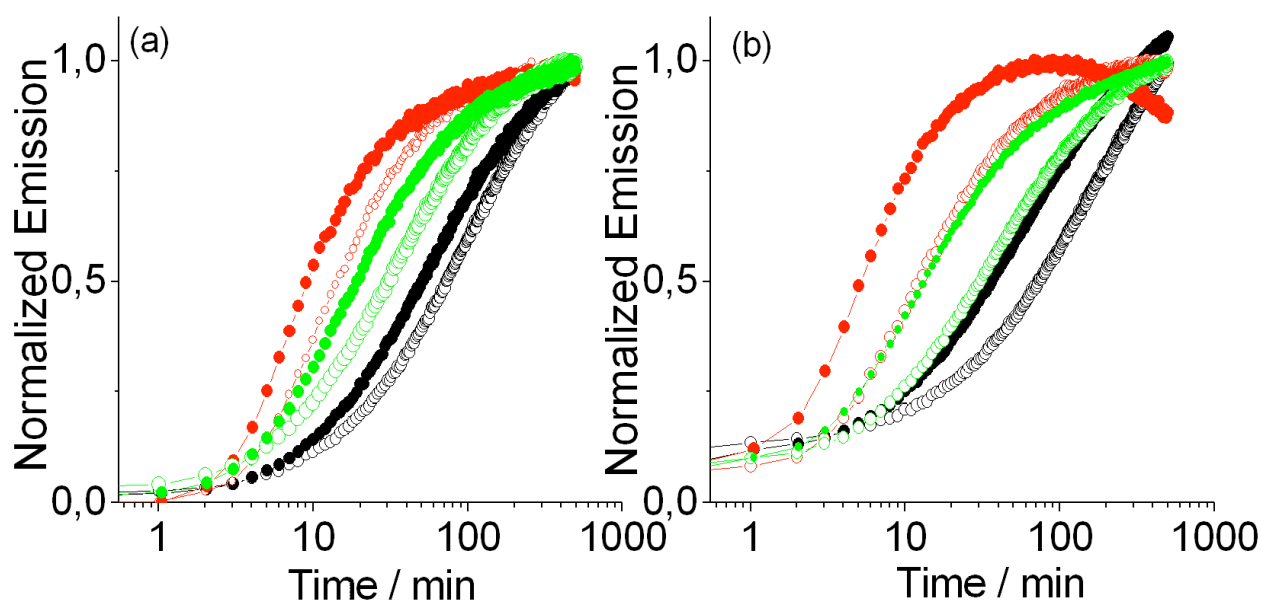


Figure 4.6: Temperature dependent threading rate after mixing $\Delta\Delta$ -P (a) and $\Lambda\Lambda$ -B (a) with ct-DNA [black = 45°C, green=50°C, red= 55°C, -o- = buffer and -●- = 10% PEG).

4.5 TA6 and $\Delta\Delta$ -P

The ct-DNA is long ($\approx 10,000$ bps) and we wanted to test if the problem with precipitation is smaller for a short DNA. Therefore the ct-DNA was sonicated to reduce the strand length to ≈ 200 -400 bps. The results for sonicated ct-DNA are good compared to ct-DNA but still showed signs of precipitation / aggregation (data not shown). Thus we used a short oligonucleotide having 20 bps with a central AT track of 12 bps and a HEG-linked hairpin (TA6). It has previously been reported that these HEG-linked oligonucleotides with variable central AT length are thermostable with a melting temperature around 65°C and that the threading rate depends on the central AT track [40].

Figure 4.7a shows threading of $\Delta\Delta$ -P into TA6 at 20°C. In contrast to ct-DNA the emission is highest in 50% PEG and lowest in buffer. There is a significant difference in emission intensity in 40% PEG compared to in buffer. To determine the threading rate the kinetic traces were normalized (figure

4.7b). The rate is highest in 50% PEG and considerably higher in 40% PEG than in buffer. Absorption spectra (figure 4.7c) were measured after kinetics and they were similar as in the literature [61]. The DNA band at 260 nm is almost identical in all PEG concentrations and buffer showing that TA6 does not aggregate or precipitate in presence of $\Delta\Delta$ -P. The steady state emission spectrum after 2000 minutes (figure 4.7d) is similar as kinetics after 1000 minutes. This means that nothing happens after 1000 minutes.

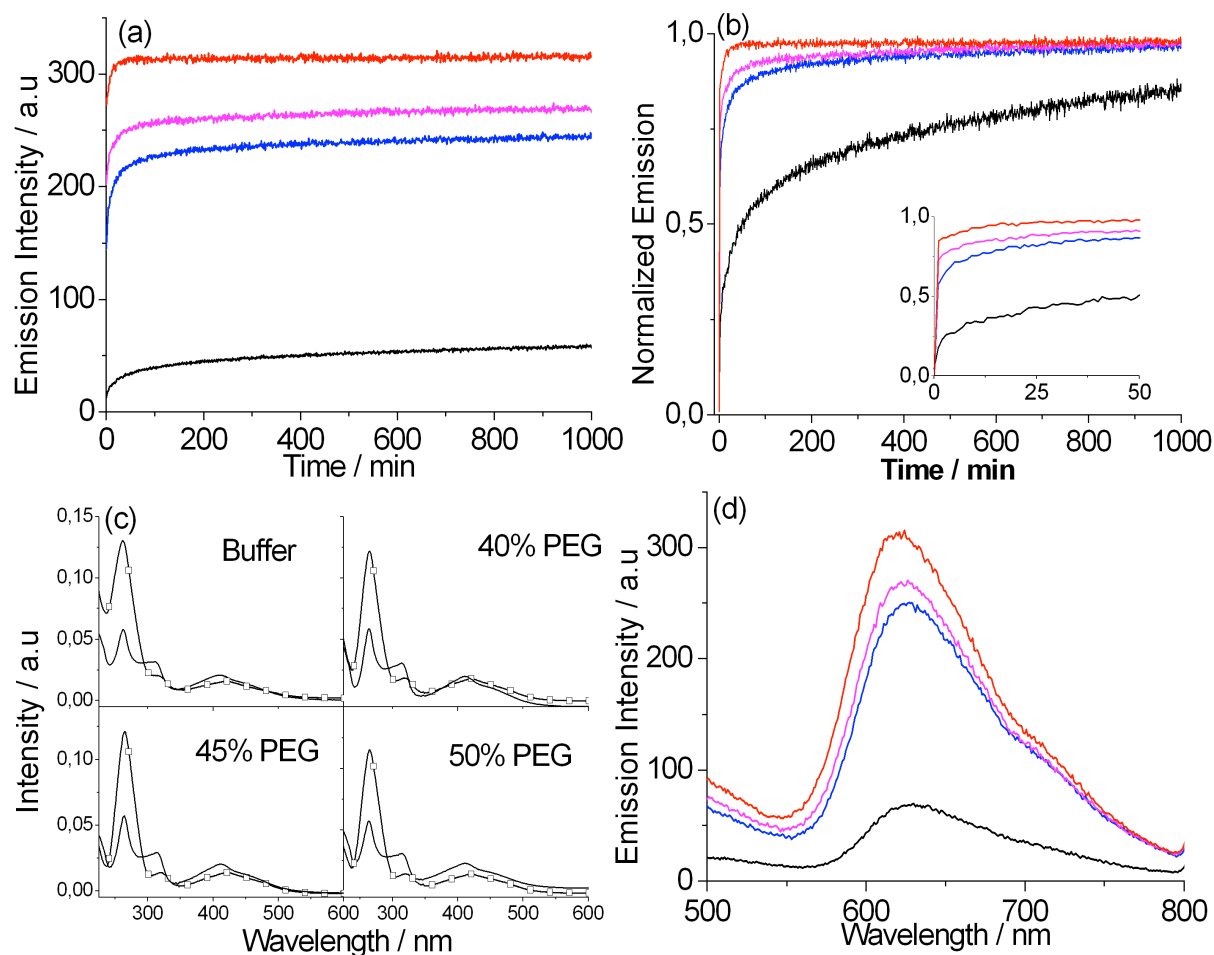


Figure 4.7: Association kinetics for $\Delta\Delta$ -P after mixing with TA6 at 20°C (a) kinetics (b) normalized kinetic traces (normalized to emission intensity after 2000 min) and inset: initial phase (c) absorption spectra before (---) and after adding DNA (-□-) (d) steady state emission spectra in different PEG concentrations (40% PEG = blue, 45% PEG = magenta and 50% PEG = red) and buffer = black. Both absorption and emission spectra are taken at room temperature.

Threading at physiological temperature (37°C) shows some additional features (figure 4.8). At this temperature we also add 30% PEG to see its effect on DNA threading. Figure 4.8a shows that the emission intensity is highest in 50% PEG and lowest in buffer. The emission is lower in 30% PEG compared to 40% PEG and higher than in buffer. The kinetic traces are normalized to the intensity after 2000 minutes. The threading appears to be slower at 37°C than 20°C, which was surprising. The inset (inset figure 4.8b) shows a very fast component that we suggest is the actual threading. The threading rate is higher in PEG compared to in buffer. The slow increase in luminescence after com-

pletion of threading is due to shuffling of complexes from one oligonucleotide to another oligonucleotide. Shuffling is prominent at high PEG concentrations (40 and 45% PEG) but not observed in 50%PEG. This shuffling was not seen at 20°C (figure 4.7). The absorption spectra (figure 4.8c) show that we have a slight aggregation of DNA compared to at 20°C in higher PEG concentrations (40-50% PEG). The steady state spectra (figure 4.8d) after 2000 minutes are similar as kinetics after 1000 minutes.

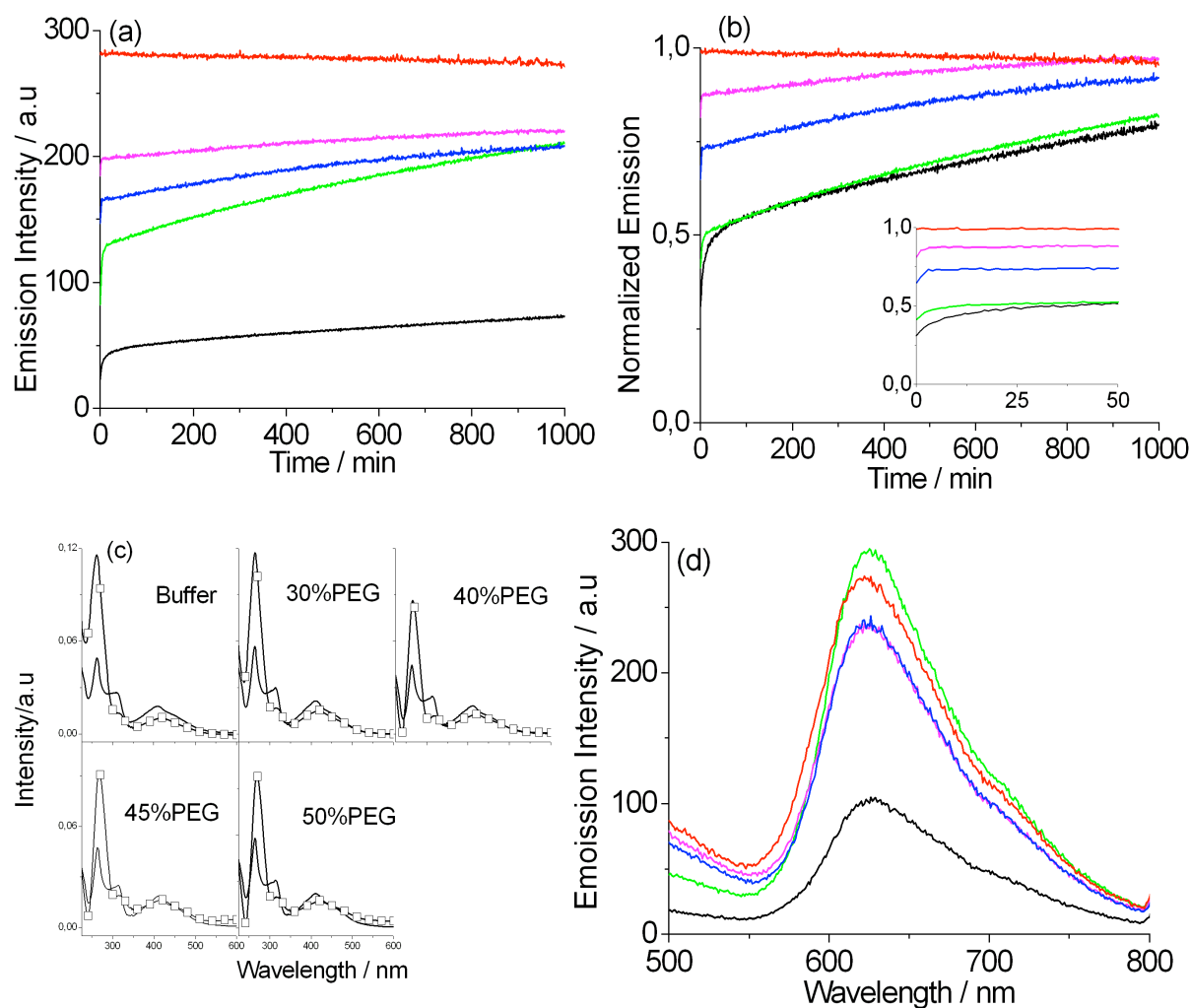


Figure 4.8: Association kinetics for $\Delta\Delta$ -P mixed with TA6 at 37°C (a) kinetic traces (b) normalized kinetic traces (normalized to emission intensity after 2000 min) and inset: initial phase (c) absorption spectra before (---) and after adding DNA (-□-). (d) Steady state emission spectra in different PEG concentrations (30% PEG = green, 40% PEG = blue, 45% PEG = magenta and 50%PEG = red) and in buffer = black. Note: Both absorption and emission spectra are taken at room temperature.

4.6 Temperature dependent threading rate for TA6

Figure 4.9 suggests that the threading rate is slower with increasing temperature but the actual threading is very fast in PEG and completed in first few minutes after addition of DNA (figure 4.9). The increase in emission after threading is due to shuffling of already threaded complexes from one oligonucleotide to another [40]. The shuffling is prominent in 40% and 45% PEG especially at higher temperatures (37 and 45°C) but no shuffling was observed in 50% PEG at any temperatures. Crowding

brings the oligonucleotides closer to each other and thus the complexes reshuffle faster (figure 4.9 f). The results of TA6 are good compared to ct-DNA. The long DNA aggregated in a crowded environment while TA6 shows much less aggregation.

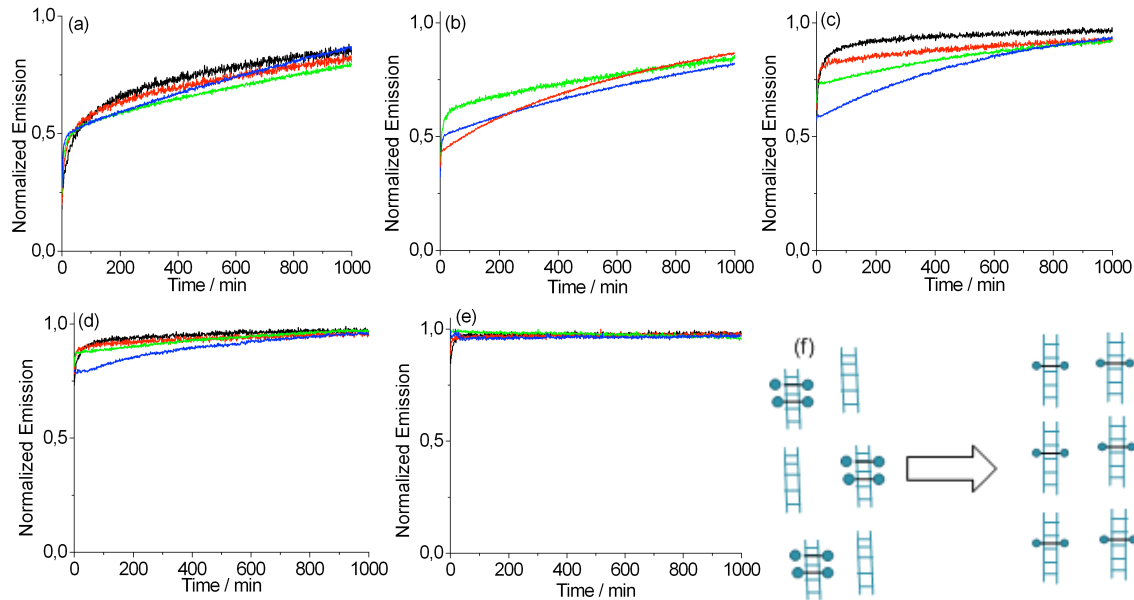


Figure 4.9: Shuffling of $\Delta\Delta$ -P after threading into TA6 at different temperatures. (a) Buffer (b) 30%PEG (c) 40% PEG (d) 45% PEG (e) 50% PEG. The kinetic traces are taken at different temperatures (20°C = black, 30°C = red, 37°C = green and 45°C = blue) (normalized to emission intensity after 2000 min). (f) Shuffling of complex between different oligonucleotides.

Figure 4.10 shows the threading rates at various temperatures at constant PEG concentration. The rate increases with increasing PEG concentration. 50% PEG has the highest and buffer has the lowest rate at all temperatures. The rate is higher at high temperature in both PEG and buffer. The rate is even faster in 50% PEG at 20°C than in buffer at 45°C. 40% PEG has significantly higher rate than buffer compare to DNA strand exchange, where buffer and 40% PEG has almost similar strand exchange rate. Probably a smaller nucleation site is required for DNA threading compared to DNA strand exchange. Therefore DNA threading is more sensitive to PEG than DNA strand exchange.

To summarize we can say that PEG catalyzes DNA threading in a similar way as it catalyzes the DNA strand exchange. The catalytic effect of PEG is due to the water activity / hydrophobic interactions because threading is believed to be only dependent on water activity and not crowding. The shuffling of the complex is due to the crowding effect of PEG.

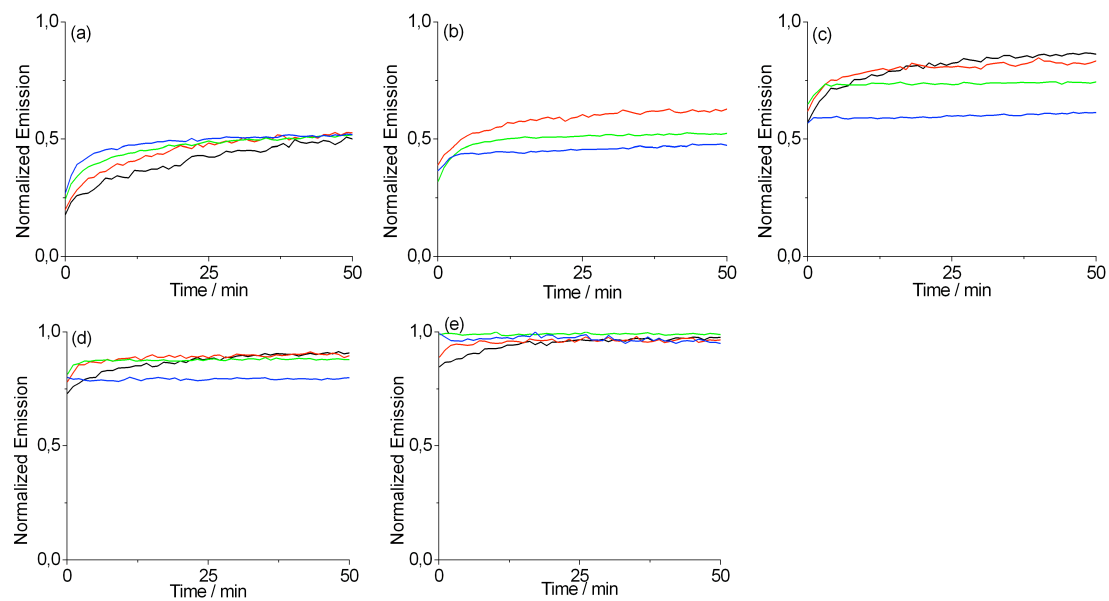


Figure 4.10: Threading of $\Delta\Delta$ -P into TA6 at different temperatures. (a) Buffer (b) 30% PEG (c) 40%PEG (d) 45% PEG (e) 50%PEG. The kinetic traces are taken at different temperatures (20°C = black, 30°C = red, 37°C = green and 45°C = blue) (normalized to emission intensity after 2000 min).

5. Conclusions and outlook

In this thesis we have investigated how PEG catalyzes DNA threading of binuclear ruthenium complexes. We use different DNA systems to study this catalysis and the following conclusions can be drawn from our results.

- A catalytic effect on DNA threading is observed for long ct-DNA at 10% PEG. At higher PEG concentrations we observe aggregation and precipitation of DNA and no solid conclusions can be drawn.
- A larger catalytic effect is observed for the less hydrophobic complex B compared to complex P. Previous dissociation studies with SDS also showed a higher catalytic effect for B compared to P. Our results show that hydrophobic interactions are important not only for dissociation but also for threading of the complex. We believe that the more hydrophobic P complex can have closer stacking contacts with exposed DNA bases in the transition state while complex B benefits more from external hydrophobic moieties.
- A short synthetic oligonucleotide (TA6) shows no or very little aggregation when P is added even at 50%PEG and the threading rate increases with increasing PEG concentration.
- There is a large catalytic effect at 40% PEG compared to in buffer for DNA threading but for DNA strand exchange the rate was almost similar in 40% PEG and in buffer. Thus threading is more sensitive to PEG compared to DNA strand exchange. The threading requires a small pocket compare to strand exchange therefore threading rate is higher in 40% PEG than in buffer.
- While DNA strand exchange can be accelerated both by crowding and hydrophobic interaction, threading should only depend on the latter. The fact that PEG catalyzes DNA threading, suggests that hydrophobic interactions are important for its catalytic activity, most likely also in the case of DNA strand exchange.
- A slow increase in emission after threading is possibly due to redistribution / shuffling of the complex between different oligonucleotides. This process is faster at higher PEG concentrations and instant at 50% PEG. Due to the crowding effect of PEG oligonucleotides can come closer to each other in space, possibly explaining why the shuffling is faster at high PEG concentrations.

In this study we have shown that PEG catalyzes DNA threading due to hydrophobic interactions. We might perform some further experiments to get a better understanding of the catalysis.

- Dynamic light scattering (DLS) is a technique which might be used to study aggregation of ct-DNA in presence of ruthenium dimers.
- PEG with different sizes (PEG 200 - 8000) has different viscosities and they behave quite differently. Therefore various PEG sizes might be used to see how they effect the threading rate.
- Other crowding agents, like dextran and Ficoll, can be used to investigate if they have the same catalytic effect as PEG to avoid specific PEG effects.
- Other complexes, such as B, can be used to investigate if they behave similar as $\Delta\Delta$ -P when threading into TA6 or if we can detect differences in catalytic activity, just as for long ct-DNA.
- Circular dichroism (CD) can be used to investigate if the DNA conformation is maintained in PEG and to confirm a threading binding mode with TA6.

To summarize, this study provides a perspective on how hydrophobic interactions affect DNA threading, which will be of interest in the design of new ruthenium-based therapeutics that target DNA.

Acknowledgement

Finally, I wish my gratitude to my supervisor and examiner Dr. Fredrik Westerlund who's consummate and indelible guidance helped me every way during the completion of this thesis. Whenever his seasoned wisdom was touched and his precious piece of advice was implored and beseeched, he was there to welcome. This thesis will incomplete with out the valuable discussion with Prof. Dr. Per Lincoln. I would like to thanks Bobo Feng; for his help during the experiments, Johanna Anderson; for kindly providing the ruthenium complexes used in this study, Pär Nordell; for discussions, Waqas Khalid; for proof reading of this thesis. I am appreciate and grateful to all the people at physical chemistry for their amiable support and favourable conduct became an unceasing delectation for me to complete this work. Last but not least, I would like to thanks my parents whose gregarious and perennial favour paved for me this way to final success.

Irfan Shaukat

Bibliography

1. Dahm, R., *Discovering DNA: Friedrich Miescher and the early years of nucleic acid research*. Human Genetics, 2008. **122**(6): p. 565-581.
2. Hershey, A.D. and M. Chase, *Independent Functions of Viral Protein and Nucleic Acid in Growth of Bacteriophage*. The Journal of General Physiology, 1952. **36**(1): p. 39-56.
3. Watson, J.D. and F.H.C. Crick, *Molecular Structure of Nucleic Acids: A Structure for Deoxyribose Nucleic Acid*. Nature, 1953. **171**(4356): p. 737-738.
4. Crick, F., *Central Dogma of Molecular Biology*. Nature, 1970. **227**(5258): p. 561-563.
5. McCarthy, B.J. and J.J. Holland, *Denatured DNA as a direct template for in vitro protein synthesis*. Proceedings of the National Academy of Sciences, 1965. **54**(3): p. 880-886.
6. Uzawa, T., A. Yamagishi, and T. Oshima, *Polypeptide Synthesis Directed by DNA as a Messenger in Cell-Free Polypeptide Synthesis by Extreme Thermophiles, Thermus thermophilus HB27 and Sulfolobus tokodaii Strain 7*. Journal of Biochemistry, 2002. **131**(6): p. 849-853.
7. Venter, J.C., et al., *The Sequence of the Human Genome*. Science, 2001. **291**(5507): p. 1304-1351.
8. *Initial sequencing and analysis of the human genome*. Nature, 2001. **409**(6822): p. 860-921.
9. Nitiss, J.L., *Targeting DNA topoisomerase II in cancer chemotherapy*. Nat Rev Cancer, 2009. **9**(5): p. 338-350.
10. Li, T.-K. and L.F. Liu, *Tumor Cell Death Induced by Topoisomerase-Targeting Drugs*. Annual Review of Pharmacology and Toxicology, 2001. **41**(1): p. 53-77.
11. Ghosh, A. and M. Bansal, *A glossary of DNA structures from A to Z*. Acta Crystallographica Section D, 2003. **59**(4): p. 620-626.
12. Wing, R., et al., *Crystal structure analysis of a complete turn of B-DNA*. Nature, 1980. **287**(5784): p. 755-758.
13. Pabo, C.O. and R.T. Sauer, *Protein-DNA Recognition*. Annual Review of Biochemistry, 1984. **53**(1): p. 293-321.
14. Bacolla, A. and R.D. Wells, *Non-B DNA Conformations, Genomic Rearrangements, and Human Disease*. Journal of Biological Chemistry, 2004. **279**(46): p. 47411-47414.
15. Chou, S.H., K.H. Chin, and A.H.J. Wang, *Unusual DNA duplex and hairpin motifs*. Nucleic Acids Research, 2003. **31**(10): p. 2461-2474.
16. Rosenberg, B., L. Van Camp, and T. Krigas, *Inhibition of Cell Division in Escherichia coli by Electrolysis Products from a Platinum Electrode*. Nature, 1965. **205**(4972): p. 698-699.
17. Giaccone, G., et al., *Gefitinib in Combination With Gemcitabine and Cisplatin in Advanced Non-Small-Cell Lung Cancer: A Phase III Trial—INTACT I*. Journal of Clinical Oncology, 2004. **22**(5): p. 777-784.
18. Rose, P.G., et al., *Concurrent Cisplatin-Based Radiotherapy and Chemotherapy for Locally Advanced Cervical Cancer*. New England Journal of Medicine, 1999. **340**(15): p. 1144-1153.
19. Guo, X.W.a.Z., *The Role of Sulfur in Platinum Anticancer Chemotherapy*. Anti-Cancer Agents in Medicinal Chemistry, 2007. **7**(1): p. 19-34
20. Sava, G. and A. Bergamo, *Ruthenium Drugs for Cancer Chemotherapy: An Ongoing Challenge to Treat Solid Tumours*, in *Platinum and Other Heavy Metal Compounds in Cancer Chemotherapy*, A. Bonetti, et al., Editors. 2009, Humana Press. p. 57-66.
21. Lentz, F., et al., *Pharmacokinetics of a novel anticancer ruthenium complex (KP1019, FFC14A) in a phase I dose-escalation study*. Anti-Cancer Drugs, 2009. **20**(2): p. 97-103
22. Antonarakis, E. and A. Emadi, *Ruthenium-based chemotherapeutics: are they ready for prime time?* Cancer Chemotherapy and Pharmacology, 2010. **66**(1): p. 1-9.

23. Polec-Pawlak, K., et al., *Application of capillary electrophoresis-inductively coupled plasma mass spectrometry to comparative studying of the reactivity of antitumor ruthenium(III) complexes differing in the nature of counter-ion toward human serum proteins*. Journal of Chromatography A, 2008. **1192**(2): p. 323-326.
24. Pongratz, M., et al., *Transferrin binding and transferrin-mediated cellular uptake of the ruthenium coordination compound KP1019, studied by means of AAS, ESI-MS and CD spectroscopy*. Journal of Analytical Atomic Spectrometry, 2004. **19**(1): p. 46-51.
25. Sorokin, L.M., E.H. Morgan, and G.C.T. Yeoh, *Transferrin receptor numbers and transferrin and iron uptake in cultured chick muscle cells at different stages of development*. Journal of Cellular Physiology, 1987. **131**(3): p. 342-353.
26. Bolhuis, A., et al., *Antimicrobial activity of ruthenium-based intercalators*. European Journal of Pharmaceutical Sciences, 2011. **42**(4): p. 313-317.
27. Navarro, M., et al., *Metal-based drugs for malaria, trypanosomiasis and leishmaniasis: recent achievements and perspectives*. Drug Discovery Today, 2010. **15**(23-24): p. 1070-1078.
28. Barton, J.K., A. Danishefsky, and J. Goldberg, *Tris(phenanthroline)ruthenium(II): stereoselectivity in binding to DNA*. Journal of the American Chemical Society, 1984. **106**(7): p. 2172-2176.
29. Matson, M., et al., *Correlation Between Cellular Localization and Binding Preference to RNA, DNA, and Phospholipid Membrane for Luminescent Ruthenium(II) Complexes*. The Journal of Physical Chemistry B, 2011. **115**(7): p. 1706-1711.
30. Hiort, C., P. Lincoln, and B. Norden, *DNA binding of Delta- and Lambda-[Ru(phen)2DPPZ]2+*. Journal of the American Chemical Society, 1993. **115**(9): p. 3448-3454.
31. Friedman, A.E., et al., *A molecular light switch for DNA: Ru(bpy)2(dppz)2+*. Journal of the American Chemical Society, 1990. **112**(12): p. 4960-4962.
32. Önfelt, B., P. Lincoln, and B. Norden, *A Molecular Staple for DNA: Threading Bis-intercalating [Ru(phen)2dppz]2+ Dimer*. Journal of the American Chemical Society, 1999. **121**(46): p. 10846-10847.
33. Wilhelmsson, L.M., et al., *DNA-Binding of Semirigid Binuclear Ruthenium Complex Δ,Δ -[μ -(11,11'-bidppz)(phen)4Ru2]4+: Extremely Slow Intercalation Kinetics*. Journal of the American Chemical Society, 2002. **124**(41): p. 12092-12093.
34. Westerlund, F., et al., *Complex DNA Binding Kinetics Resolved by Combined Circular Dichroism and Luminescence Analysis*. The Journal of Physical Chemistry B, 2008. **112**(21): p. 6688-6694.
35. Lincoln, P. and B. Norden, *Binuclear ruthenium(II) phenanthroline compounds with extreme binding affinity for DNA*. Chemical Communications, 1996(18): p. 2145-2146.
36. Paramanathan, T., et al., *Mechanically manipulating the DNA threading intercalation rate*. Journal of the American Chemical Society, 2008. **130**(12): p. 3752-3.
37. Westerlund, F., et al., *Kinetic characterization of an extremely slow DNA binding equilibrium*. The Journal of Physical Chemistry B, 2007. **111**(30): p. 9132-7.
38. Nordell, P., et al., *Kinetic recognition of AT-rich DNA by ruthenium complexes*. Angewandte Chemie-International Edition 2007. **46**(13): p. 2203-6.
39. Andersson, J., M. Li, and P. Lincoln, *AT-Specific DNA Binding of Binuclear Ruthenium Complexes at the Border of Threading Intercalation*. Chemistry – A European Journal, 2010. **16**(36): p. 11037-11046.
40. Nordell, P., et al., *DNA polymorphism as an origin of adenine-thymine tract length-dependent threading intercalation rate*. Journal of the American Chemical Society, 2008. **130**(44): p. 14651-8.
41. Gardner, M.J., et al., *Genome sequence of the human malaria parasite Plasmodium falciparum*. Nature, 2002. **419**(6906): p. 498-511.

42. Marcus, R.A., *Micelle-Enhanced Dissociation of a Ru Cation /DNA Complex*. The Journal of Physical Chemistry B, 2005. **109**(45): p. 21419-21424.
43. Westerlund, F., et al., *Micelle-Sequestered Dissociation of Cationic DNA-Intercalated Drugs: Unexpected Surfactant-Induced Rate Enhancement*. Journal of the American Chemical Society, 2003. **125**(13): p. 3773-3779.
44. Zimmerman, S.B. and L.D. Murphy, *Macromolecular crowding and the mandatory condensation of DNA in bacteria*. FEBS Letters, 1996. **390**(3): p. 245-248.
45. Chebotareva, N.A., B.I. Kurganov, and N.B. Livanova, *Biochemical effects of molecular crowding*. Biochemistry (Moscow), 2004. **69**(11): p. 1239-1251.
46. Miyoshi, D. and N. Sugimoto, *Molecular crowding effects on structure and stability of DNA*. Biochimie, 2008. **90**(7): p. 1040-1051.
47. Zhou, H.-X., G. Rivas, and A.P. Minton, *Macromolecular Crowding and Confinement: Biochemical, Biophysical, and Potential Physiological Consequences**. Annual Review of Biophysics, 2008. **37**(1): p. 375-397.
48. Ellis, R.J., *Macromolecular crowding: obvious but underappreciated*. Trends in Biochemical Sciences, 2001. **26**(10): p. 597-604.
49. Minton, A.P., *How can biochemical reactions within cells differ from those in test tubes?* J Cell Sci, 2006. **119**(14): p. 2863-2869.
50. Minton, A.P., *Implications of macromolecular crowding for protein assembly*. Current Opinion in Structural Biology, 2000. **10**(1): p. 34-39.
51. Kidoaki, S. and K. Yoshikawa, *Folding and unfolding of a giant duplex-DNA in a mixed solution with polycations, polyanions and crowding neutral polymers*. Biophysical Chemistry, 1999. **76**(2): p. 133-143.
52. Tsao, D., A.P. Minton, and N.V. Dokholyan, *A Didactic Model of Macromolecular Crowding Effects on Protein Folding*. PLoS ONE, 2010. **5**(8): p. e11936.
53. Cheung, M.S., D. Klimov, and D. Thirumalai, *Molecular crowding enhances native state stability and refolding rates of globular proteins*. Proceedings of the National Academy of Sciences of the United States of America, 2005. **102**(13): p. 4753-4758.
54. Kudlay, A., M.S. Cheung, and D. Thirumalai, *Crowding Effects on the Structural Transitions in a Flexible Helical Homopolymer*. Physical Review Letters, 2009. **102**(11): p. 118101.
55. He, S., P.G. Arscott, and V.A. Bloomfield, *Condensation of DNA by multivalent cations: Experimental studies of condensation kinetics*. Biopolymers, 2000. **53**(4): p. 329-341.
56. Nakano, S.-i., et al., *Conformation and the sodium ion condensation on DNA and RNA structures in the presence of a neutral cosolute as a mimic of the intracellular media*. Molecular BioSystems, 2008. **4**(6): p. 579-588.
57. Nakano, S.-i., et al., *The Effect of Molecular Crowding with Nucleotide Length and Cosolute Structure on DNA Duplex Stability*. Journal of the American Chemical Society, 2004. **126**(44): p. 14330-14331.
58. Feng, B., et al., *DNA strand exchange catalyzed by molecular crowding in PEG solutions*. Chemical Communications, 2010.
59. Wilhelmsson, L.M., et al., *Meso Stereoisomer as a Probe of Enantioselective Threading Intercalation of Semirigid Ruthenium Complex $[\mu-(11,11'\text{-bidppz})(\text{phen})_4\text{Ru}_2]^{4+}$* . The Journal of Physical Chemistry B, 2003. **107**(42): p. 11784-11793.
60. Per Lincoln, B.N., *Binuclear complex*. US, Patent (6440971), 2002.
61. Westerlund, F., et al., *Binding geometry and photophysical properties of DNA-threading binuclear ruthenium complexes*. J Phys Chem B, 2007. **111**(1): p. 310-7.
62. Westerlund, F. and P. Lincoln, *AT-dependent luminescence of DNA-threading ruthenium complexes*. Biophysical Chemistry, 2007. **129**(1): p. 11-7.

63. Westerlund, F., et al., *Enantioselective luminescence quenching of DNA light-switch [Ru(phen)2dppz]2+ by electron transfer to structural homologue [Ru(phendione)2dppz]2+*. *The Journal of Physical Chemistry B*, 2005. **109**(36): p. 17327-32.
64. Westerlund, F., et al., *Complex DNA binding kinetics resolved by combined circular dichroism and luminescence analysis*. *Journal of Physical Chemistry B*, 2008. **112**(21): p. 6688-6694.